

## Chapter 3

# LA-Azusa Aerosol Evolution

### 3.1 Introduction

The generation and evolution of particulate matter in southern California may be examined by comparing the samples from two or more sites that lie along common wind trajectory paths (Hughes 2000; Hughes 1999; Gard 1998 and references therein). During late August of 1997, three ATOFMS instruments were located in Los Angeles, Azusa, and Riverside, CA. The transportable instruments sampled in Los Angeles and Azusa during the month of August 1997 and the lab-based ATOFMS sampled in Riverside throughout the SCOS97-NARSTO study. On Thursday, August 21 trajectory calculations indicate that air parcels traveled along the anticipated site-to-site path from central Los Angeles to Azusa (Figure 3.1).

### 3.2 Experimental methods

As discussed in Section 2.3, ATOFMS was used to characterize individual ambient aerosol particles. The ATOFMS data are calibrated for size and the time axes are converted to the corresponding  $m/z$  values. The data are compiled in the YAADA database (see Chapter 2 for details). Digital mass spectra provide a way to display the trends in a set of single particle mass spectra. For each mass spectrum in the dataset, each  $m/z$  ( $m/z$ ) is checked to see if there is a peak (based on a specified threshold for peak height or area). This creates for each particle a series of ones (presence) and zeros (absence) for each  $m/z$ . The ones and zeros for each  $m/z$  are summed over all the mass spectra in the dataset and divided by the number of mass spectra. This indicates the fraction of the particles that produced spectra with an ion peak above the set threshold for each  $m/z$ . The digital mass spectrum plots this fraction of particles versus  $m/z$ , in which  $y$  = fraction of single particle mass spectra containing an ion peak at each  $m/z$  ( $x$ ). These digital mass spectra represent the mass spectra as a presence/absence.

As discussed in Chapter 2, the neural network ART-2a analysis can be applied to ATOFMS data. In this chapter, the existing Riverside clusters are incorporated in this analysis rather than creating new classes or clusters for these ambient particles, as previously demonstrated and detailed in Chapter 2. Matching ambient particles to existing classes from Riverside indicates which ambient particles have compositions similar to the particles from Riverside and which particles cannot be matched to existing classes. These “unmatched” particles represent new or uncommon chemical compositions. The neural network will use the “unmatched” particles to create new classes.

Air parcel trajectory plots, created by backward integration through hourly wind fields, were calculated from the wind speed and direction observations in the region (Figure 3.1). The Cass research group at Caltech generated these trajectory plots using the method of Goodin et al., as discussed in Section 2.3. To examine the same air mass at multiple sites, these trajectories were used to select data from appropriate times at each site for comparison. Because the

ATOFMS data are collected for individual particles in real time, the database can be easily searched over the time range of interest.

### 3.3 Results and Discussion

#### 3.3.1 Air Mass Trajectories for Transport from Los Angeles to Azusa

During the discussed time period, the winds directed the same air mass over the central Los Angeles and Azusa sampling sites. Two distinct transport examples are discussed here. The air parcel that arrived at Azusa in the late evening of August 21, 1997 passed near the Los Angeles sampling site in the early afternoon of the same day, moving quickly over the region (“trajectory 1”). The particles sampled by the transportable ATOFMS instrument in Los Angeles on August 21, 1997 12:40-15:40 and in Azusa on August 21, 1997 17:30-22:30 were likely sampled from the same air mass. The model estimates the time-over-land for the air mass (see Figure 3.1, top map). The early afternoon Los Angeles air mass had spent only ~2.5 hours over land. Once the air mass reached Azusa in the late evening it had spent ~7.5 hours over land. Another air mass arrived at the Azusa site in the morning of August 22, 1997, having previously passed near the Los Angeles sampling site in the late afternoon and early evening of the previous day, August 21, 1997 (“trajectory 2”). The particles sampled in Los Angeles on August 21, 1997 15:30-18:30 and in Azusa on August 22, 1997 8:00-11:00 were likely taken from the same air mass (see Figure 3.1, lower map). The late afternoon Los Angeles air mass had also spent only ~2.5 hours over land. However, once the air mass reached Azusa in the late evening, it had spent ~19 hours overland, stagnating near Azusa overnight. The transformations of the particles in the air masses are discussed in this chapter to demonstrate how single particle data can be used to understand atmospheric transformation processes occurring on individual particles.

#### 3.3.2 Chemical Composition Overview Using Digital Mass Spectra for Trajectory 1

While the overall size histograms for these times and locations are similar, the digital mass spectra for trajectory 1 clearly indicate the appearance of new peaks (i.e.  $m/z$  86 and 118) in Figure 3.2 and 3.3 as the air mass moved from Los Angeles to Azusa. These digital mass spectra are based on the unscaled ATOFMS data and thus are shown for qualitative comparisons to determine chemical differences between the two time periods. The peaks at 86 and 118 are markers for alkylamines. A likely peak assignment for the ions in these mass spectra is  $^{86}[(C_2H_5)_2N=CH_2]^+$ , a commonly observed fragment of alkylamines detected in ATOFMS smog chamber experiments. These species are formed in particles by secondary processing of particles in analogy to gaseous nitric acid combining with ammonia. Specifically, in this case, gas phase amines react with nitric acid forming an ammonium salt in the particles. Possible sources of the amines include vehicle exhaust (from additives) and agricultural areas (Angelino 2001). These results indicate that the amine signatures in the ambient particles can be used to indicate aging and secondary reactions. The size profiles of the organic carbon with amine particle type show a slight shift in particle size, reflecting particle growth (see discussion below regarding matching classes and Figure 3.8).

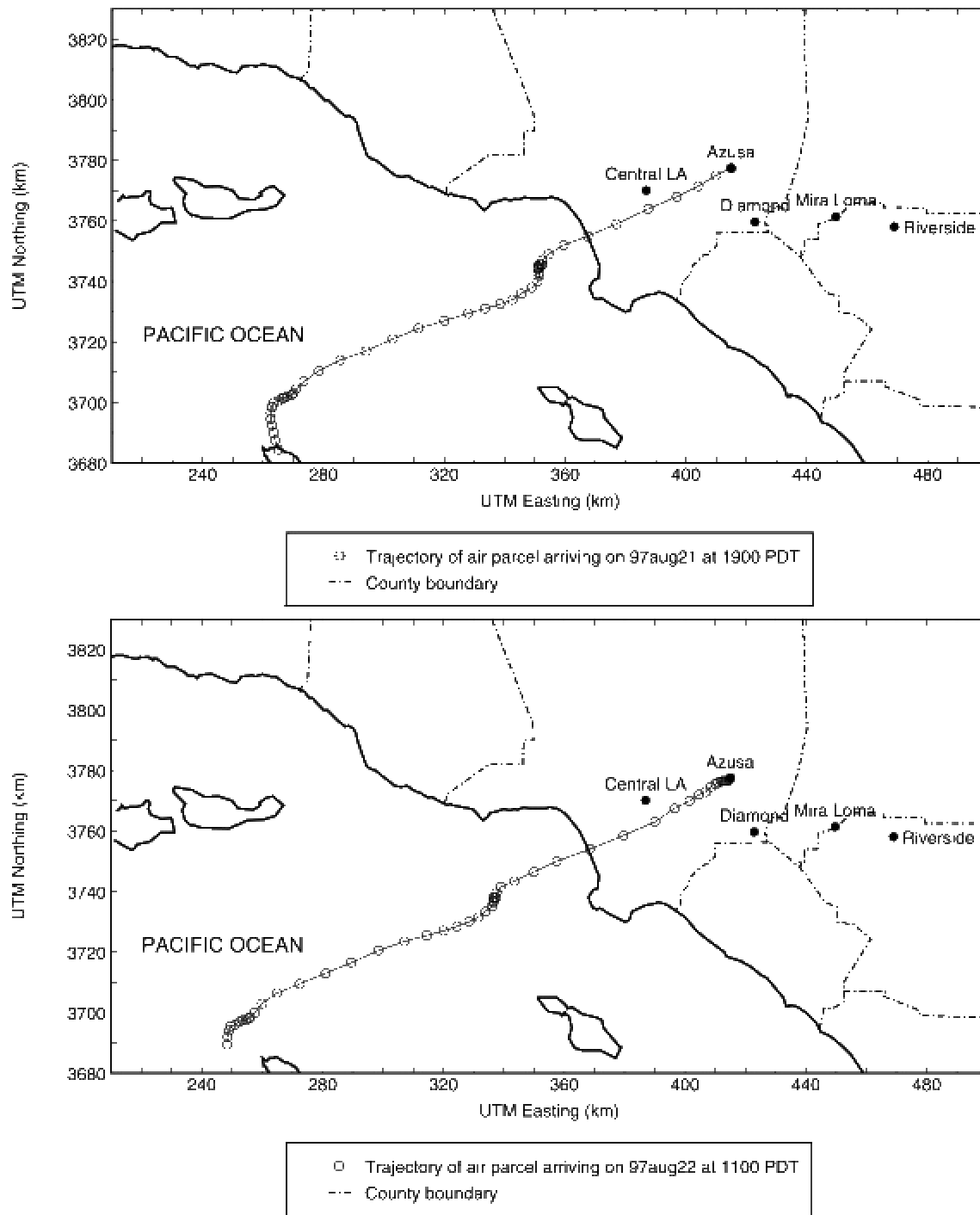


**Figure 3.1: Maps of ATOFMS sampling sites for SCOS97-NARSTO showing the air parcel trajectories for two air masses passing near Los Angeles and arriving in Azusa, CA during SCOS97-NARSTO.**

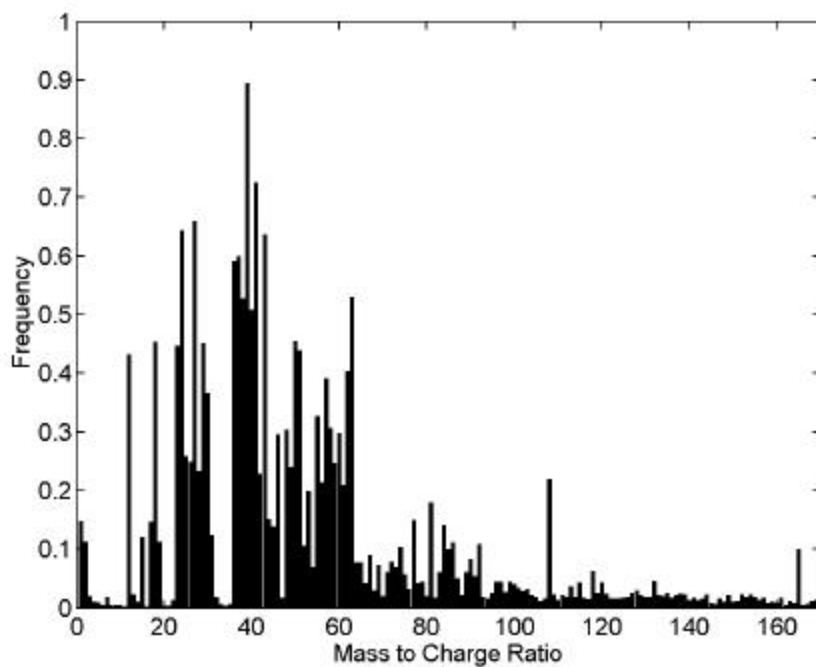


**Figure 3.2: Positive ion digital mass spectrum of particles sampled in Los Angeles, CA on August 21, 1997.**

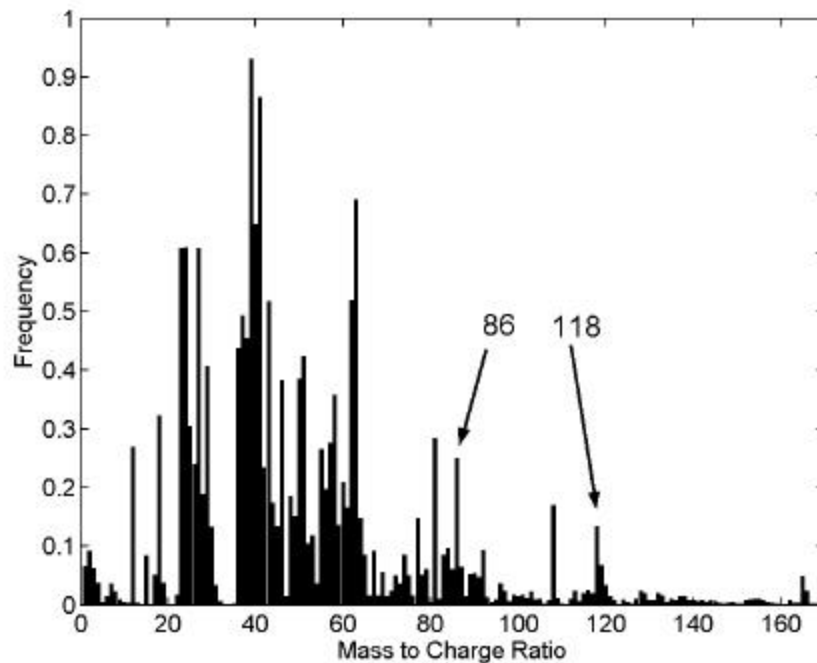


**Figure 3.3: Positive ion digital mass spectrum of particles sampled in Azusa, CA on August 21, 1997. These particles are part of the same air mass as those sampled in Los Angeles (see Figure 3.2).**

### 3.3.3 Chemical Class Comparison to Riverside

For classification, the particles from Los Angeles and Azusa can be compared to the types measured in Riverside. In order to allow direct comparison between particle types (and relative numbers) for the different sites studied across the basin, the clusters generated when analyzing Riverside particles (Ch. 2) are used for this analysis. Taking advantage of the previous ART-2a classification results provides a number of advantages. For example, the process of matching particles to existing classes is faster than creating new classes. The class interpretation is minimized because the size and composition of the classes were previously characterized. Perhaps most importantly, we can scan the data from new datasets (in this case for new sites) for particles with similar composition to the particles originally used to make the classes. This allows the particles at multiple times/sites to be compared directly. The top ranking 20 clusters explain over 99% of the ambient particles observed in Riverside. When the “trajectory 1” data from Los Angeles and Azusa are matched (vigilance factor 0.5) to these same Riverside classes, about 92% of the particles can be explained by the same general classes if only the positive ion mass spectra are considered. The unmatched particles were run through ART-2a to see if new classes were added but none of the new classes contained more than 20 particles.

The size-composition relationships observed in Riverside show a separation in major particle types based on chemical differences at about 1  $\mu\text{m}$ . Thus, the particles from Los Angeles and Azusa were separated into two size ranges, sub- and super- $\mu\text{m}$ . As anticipated, particle classes such as sea salt (clusters 1 and 2) occurred in the super- $\mu\text{m}$  range, while organic carbon (such as cluster 4) classes were predominately in the sub- $\mu\text{m}$  range. This is illustrated in Figures 3.4-3.7. For a numerical summary of the results, see Appendices D and E.

To visualize the changes in the percent of particles that match each class as the air mass moved inland, Figures 3.8-3.11 directly compare the matching results between two sites. The y-axis is the difference in percent of particles per class. The classes with positive-going bars are more prevalent at the site listed in the upper portion of the plot compared to the site listed in the lower portion. The sites in Los Angeles and Azusa for “trajectory 1” are compared in Figures 3.8 and 3.9. In addition, Azusa during “trajectory 1” is compared to Riverside (the average composition for August 21-23, 1997) in Figures 3.10 and 3.11. The sub- $\mu\text{m}$  particles are found most commonly in clusters 4, 11, 16, and 17. Clusters 4 and 11 can be briefly described as organic carbon with amines. Amines accumulate on particles by secondary processing of the particles as described in Section 3.3.2. The core of these particles resembles particles sampled from gasoline (light duty) vehicles in recent source characterization studies. However, these particles have accumulated ammonium, nitrates, and amines. Clusters 16 and 17 show a signature representative of elemental carbon formed in fresh vehicular emissions. As the air mass moves from Los Angeles to Azusa, a larger percentage of the detected particles are classified in clusters 4 and 11, clusters suggesting secondary processing of primary vehicle particles. In addition, the vanadium-rich cluster 14 is more commonly detected in Azusa as well as calcium-rich cluster 6. The diminishing population of clusters 7, 12, 16, and 17 offsets the particle composition shift toward clusters of organic carbon with amines (aged vehicle exhaust), vanadium-rich, and calcium-rich compositions. The fresh freeway emission may have resulted in clusters 16 and 17 being more common at the Central Los Angeles site (located near the 110, 5, and 101 freeways) in contrast to the more suburban Azusa location. Soil-dust, clusters 18-20, potassium-rich (clusters 5 and 7), and calcium-rich (cluster 6) are more populated in Azusa. The

nearby quarry accounts for much (if not all) of the additional soil-dust component in the Azusa aerosol as the quarry activities suspended soil particles in the area during the study.

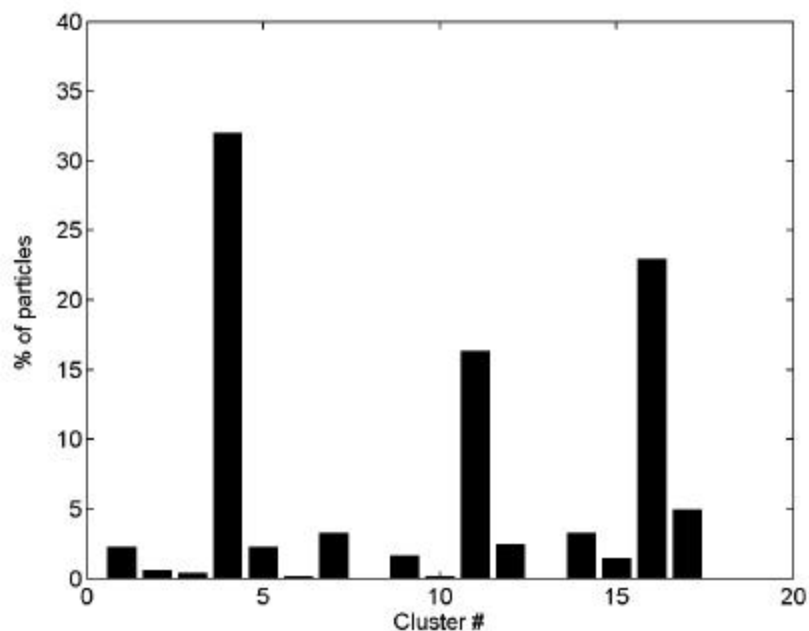


**Figure 3.4: Number of sub-mm particles per class, identified by ART-2a (vigilance, 0.5; learning 0.05; 20 iterations, classes generated from Riverside data). Particles sampled by the ATOFMS in Los Angeles, CA on August 21, 1997.**

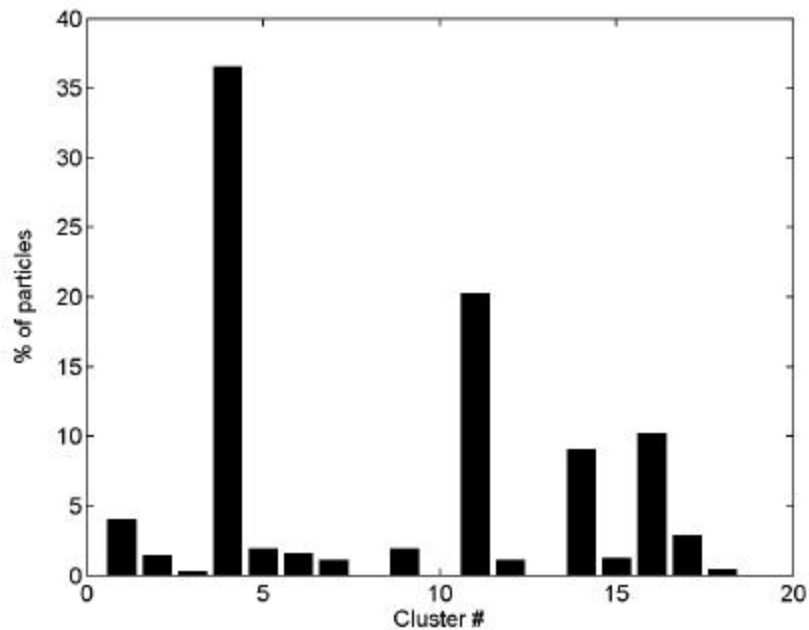


**Figure 3.5: Number of sub-mm particles per class, identified by ART-2a (vigilance, 0.5; learning 0.05; 20 iterations, classes generated from Riverside data). Particles sampled by the ATOFMS in Azusa, CA on August 21, 1997.**

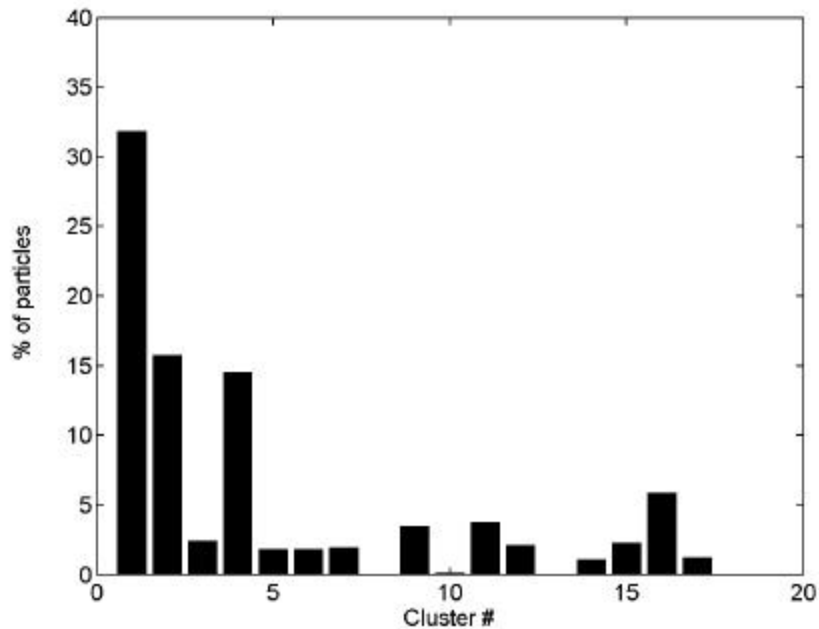


**Figure 3.6: Number of super-mm particles per class, identified by ART-2a (vigilance, 0.5; learning 0.05; 20 iterations, classes generated from Riverside data). Particles sampled by the ATOFMS in Los Angeles, CA on August 21, 1997.**

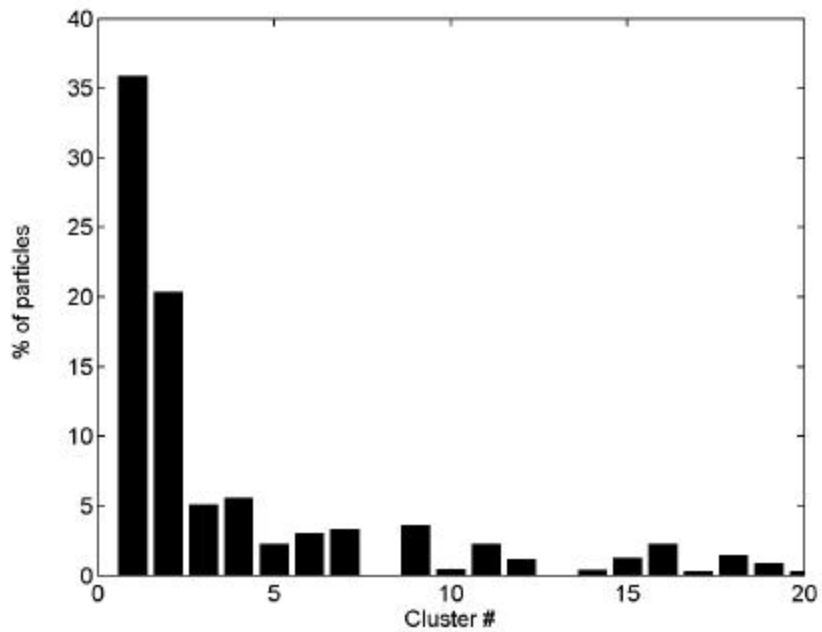


**Figure 3.7: Number of super-mm particles per class, identified by ART-2a (vigilance, 0.5; learning 0.05; 20 iterations, classes generated from Riverside data). Particles sampled by the ATOFMS in Azusa, CA on August 21, 1997.**

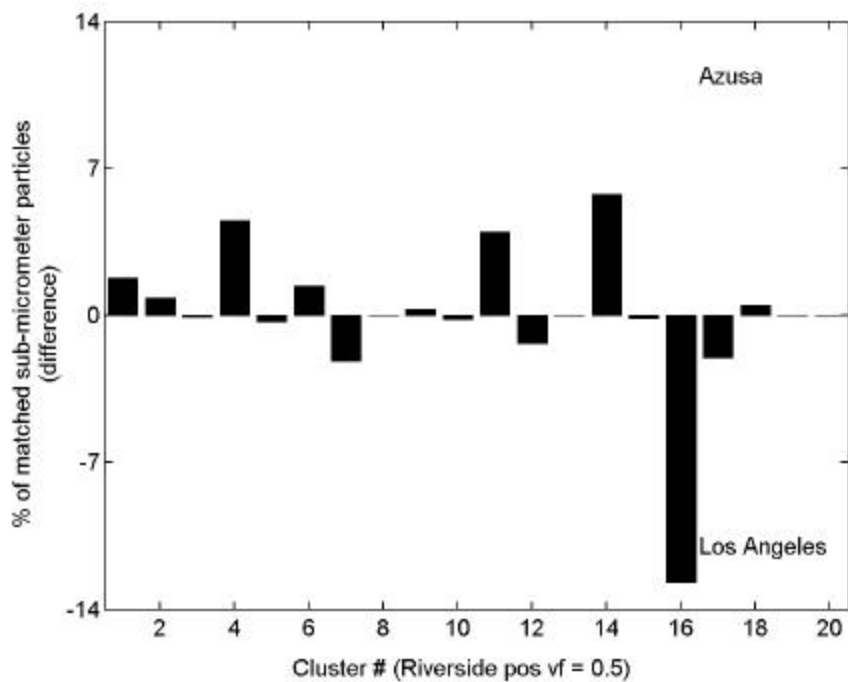


**Figure 3.8: Difference in the percent of sub-mm particles matched per ART-2a class, (y-axis: Azusa - Los Angeles. Particles sampled by the ATOFMS in Los Angeles and Azusa, CA on August 21, 1997 along “trajectory 1”.**

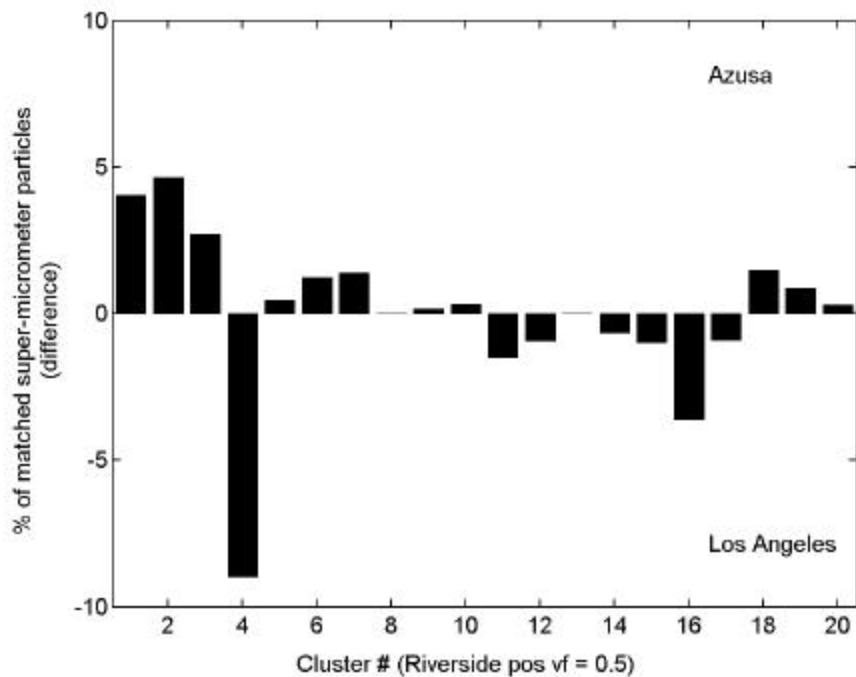


**Figure 3.9: Difference in the percent of super-mm particles matched per ART-2a class (y-axis: Azusa minus Los Angeles. Particles sampled by the ATOFMS in Los Angeles and Azusa, CA on August 21, 1997 along “trajectory 1”.**

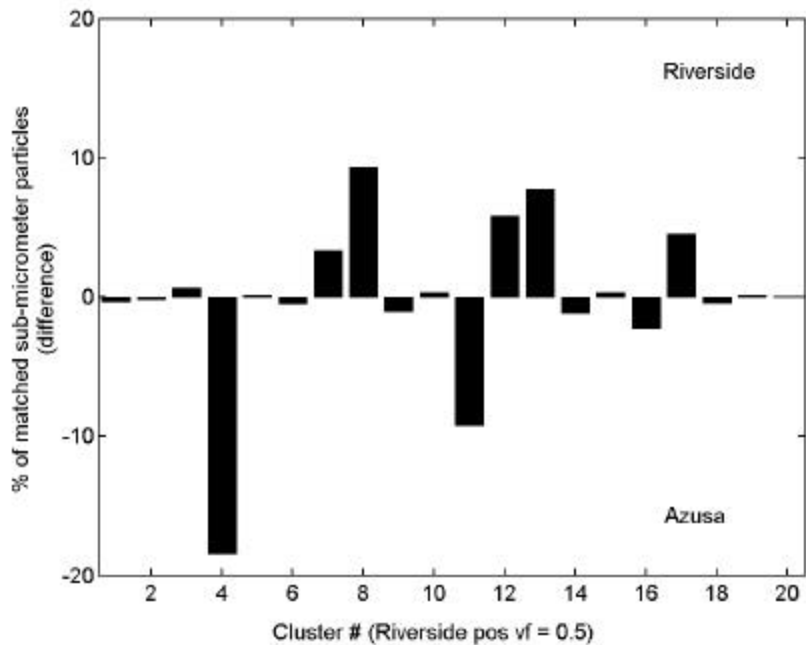


**Figure 3.10: Difference in the percent of sub-mm particles matched per ART-2a class, (y-axis: Riverside - Azusa). Particles sampled by the ATOFMS in Azusa on August 21, 1997 along “trajectory 1” and Riverside, CA during August 21-23, 1997.**

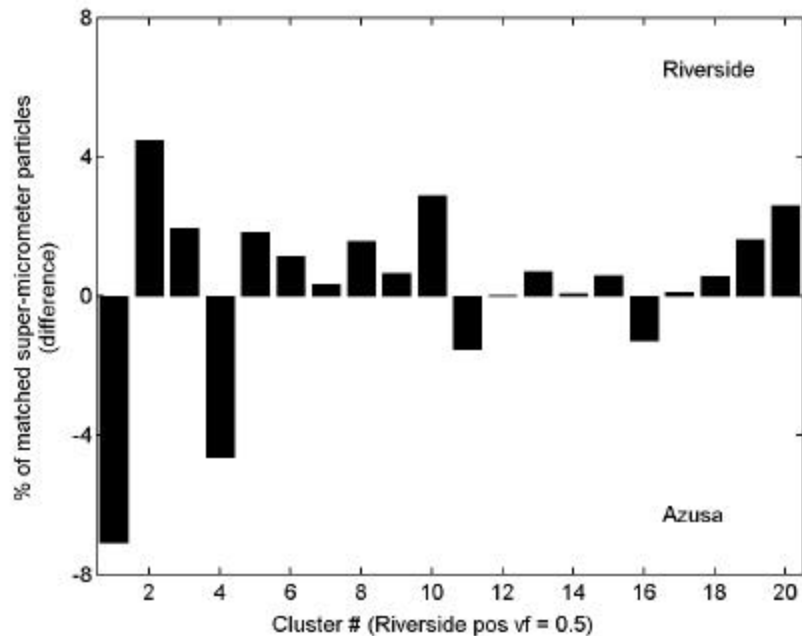


**Figure 3.11: Difference in the percent of super-mm particles matched per ART-2a class (y-axis: Riverside - Azusa). Particles sampled by the ATOFMS in Azusa in August 21, 1997 along “trajectory 1” and Riverside, CA during August 21-23, 1997.**

As the air mass moved from the mid-region site, Azusa, to a further inland site, Riverside, there were additional changes in the particle composition. The sub-  $\mu\text{m}$  ammonium-nitrate-rich cluster 8, 12, and 13 became more abundant, as did the number of particles in carbon cluster 17. The percentages of particles matched to the super-  $\mu\text{m}$  soil dust classes, clusters 10 and 18-20, further increase, as do particles in the more reacted sea salt cluster 2. Clusters 4 and 11, amine-rich organic carbon, remain most closely associated with the Azusa site, as does the less reacted sea salt cluster 1.

Depending on the site and meteorological conditions, such as relative humidity at the time of sampling, the size-composition break may not always occur at exactly 1  $\mu\text{m}$ . In order to examine this further, the size distribution of the particle types of interest can be plotted. At times, the distribution will show just a slight shift due to a few (normally) sub-  $\mu\text{m}$  type particles having sizes just over 1  $\mu\text{m}$  in aerodynamic diameter. At other times, the major components that typically appear in sub-  $\mu\text{m}$  types appear as a coating on super-  $\mu\text{m}$  type particles.

Particle vaporization is dependent on several factors including particle size, water content of the particle, laser irradiance, and the ability of the species in the particle to absorb energy at the wavelength of the desorption/ionization laser. While some super-  $\mu\text{m}$  particles appear to be completely vaporized, others appear to undergo incomplete particle vaporization, leading to the observation of coated species (i.e. organics, ammonium, nitrate, amines) over core inorganic species. This preferential vaporization of the surface material of a coated particle results in an observed particle composition biased toward the coating composition. A super-  $\mu\text{m}$  partially vaporized particle may be mis-classified as a sub-  $\mu\text{m}$  particle type if that class' composition best matches the composition of the coating. Experiments to understand and optimize particle vaporization continue in our lab as well as other groups in the field of single particle mass spectrometry (Woods 2002). These studies include testing a variety laser wavelengths and powers. In this field study, all ATOFMS instruments used 266 nm desorption/ionization lasers and the laser irradiances remained unchanged ( $\sim 1$  mJ) during the study.

The size distributions of the particles classified as clusters 4 and 11 are displayed in Figure 3.12 for Los Angeles and Azusa trajectory 1 (August 21, 1997 12:40-15:40 and 17:30-22:30, respectively). There is a slight shift in the sub- $\mu\text{m}$  mode toward larger sizes for Azusa, as compared to Los Angeles, indicating the particles accumulating secondary species during transport.

### **3.3.4 Chemical Composition Overview Using “Stacked” Digital Mass Spectra of Classes for Trajectory 1**

Another descriptive plot that can be generated for Los Angeles and Azusa is a digital mass spectrum of the particles falling in each class. The digital mass spectra may be enhanced to include a representation of relative intensity by including a pattern code for each bar plotted, or a “stacked” digital mass spectrum. Within each bar, different patterns are used to indicate the intensity of the peaks, while the height represents the relative fraction of particle spectra with each peak. For these plots, the necessary threshold for considering a peak as “present” is 1 % of the relative area (ion intensity for peak of interest/total ion intensity of all peaks in mass spectrum) of the mass spectrum must occur at that particular  $m/z$ . The 1% is arbitrary and can be varied based on the particular dataset. For example, if the total integrated area of a spectrum is 1,000 (100%), the area between  $m/z$  11.5 and 12.5 would have to be greater than or equal to 1% (or 10 area units) of the total area for a peak to be considered present at  $m/z$  12. If 1-4% of the

area occurs at a given  $m/z$ , the portion of that bar from that particle is a striped pattern. If 4-8% of the area occurs at a given  $m/z$  the portion of the bar representing the

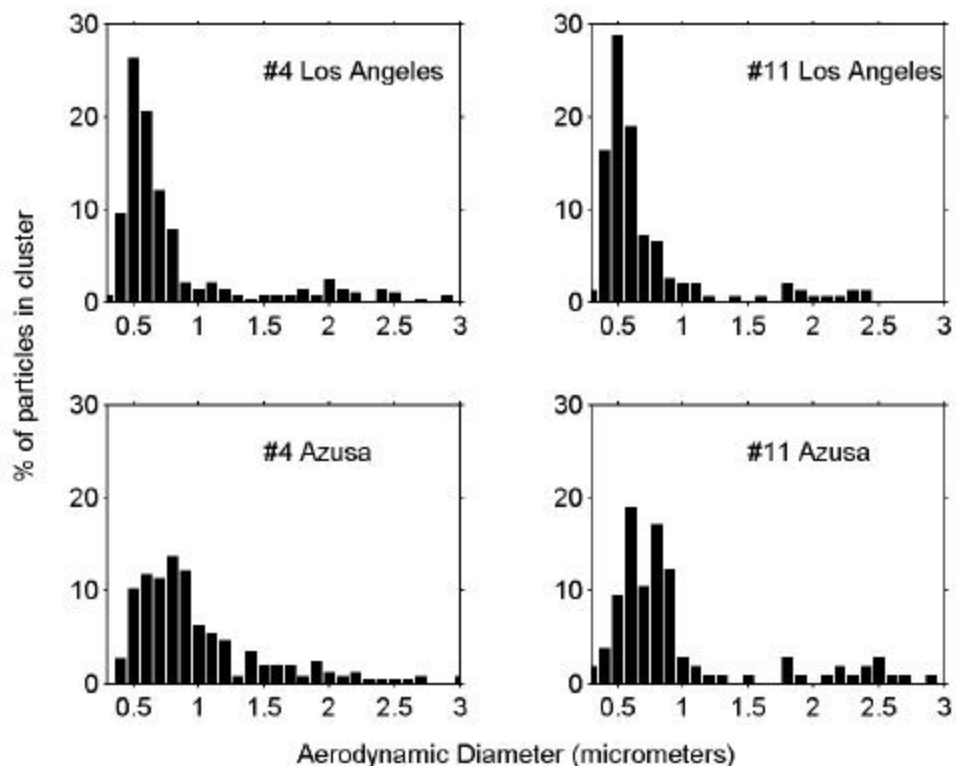


**Figure 3.12: Size distribution plots for particles matched to the common organic particles, identified by ART-2a (vigilance, 0.5; learning 0.05; 20 iterations, classes generated from Riverside data). Particles sampled by the ATOFMS in Azusa, CA on August 21, 1997.**

contribution of that particle is white, for 8-12 % the portion is gray, and for >12% the portion is filled with a cross pattern.

For both Los Angeles and Azusa, the “stacked” digital mass spectra are shown for organic carbon-ammonium nitrate cluster 4 in Figures 3.13 and 3.14. The appearance of peaks at  $m/z$  86 and 118 is evident, with some mass spectra having more than 4% of the relative area in these peaks. Other peaks in the spectra, including  $m/z$  27, 37, and 58, also are common in these organic carbon particles. The relative areas of  $m/z$  12 and 36 ion peaks are higher in LA, indicating the higher abundance of fresh (elemental carbon) emissions. There is slightly more signal at  $m/z$  27 and 37 in Azusa than in Los Angeles and  $m/z$  58 stands out as having increased in the overall number of particles as well as the intensity of the peak. Since  $m/z$  58 is a fragment of the amines, it shows an increase with an increase in  $m/z$  86 and 118. Similar plots for other clusters also indicate differences in the Los Angeles and Azusa data. Interestingly, the elemental carbon cluster 17 for Azusa also shows some amine-enriched character. The Riverside classes do not allow for differentiation between these dissimilar particle types into different classes. Also, since the transportable instruments acquired both positive and negative ion mass spectra (dual ion), there is the potential to further discriminate between the classes in two ways. The data can be analyzed by using a higher vigilance factor as well as by using both the positive and negative ions as inputs.

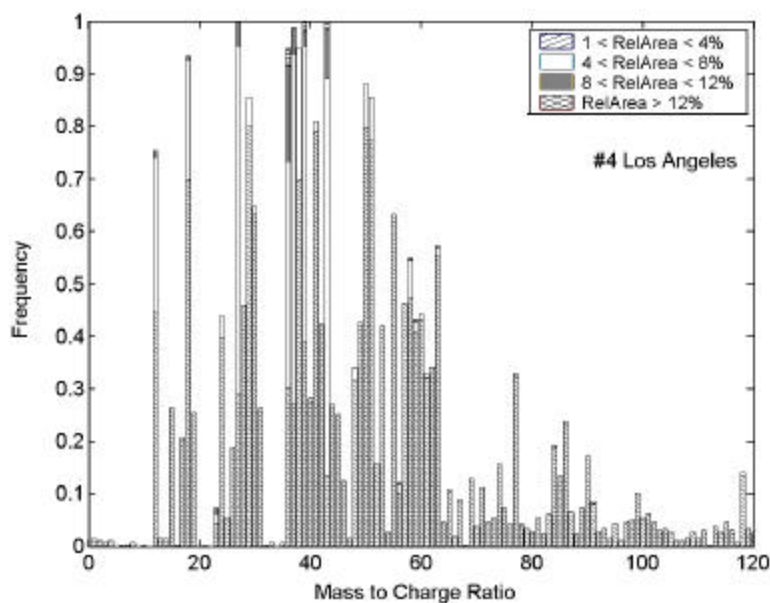


**Figure 3.13: Positive ion “stacked” digital mass spectrum of particles sampled in Los Angeles, CA on August 21, 1997 and matched to the Riverside cluster 4 organic carbon with amines.**

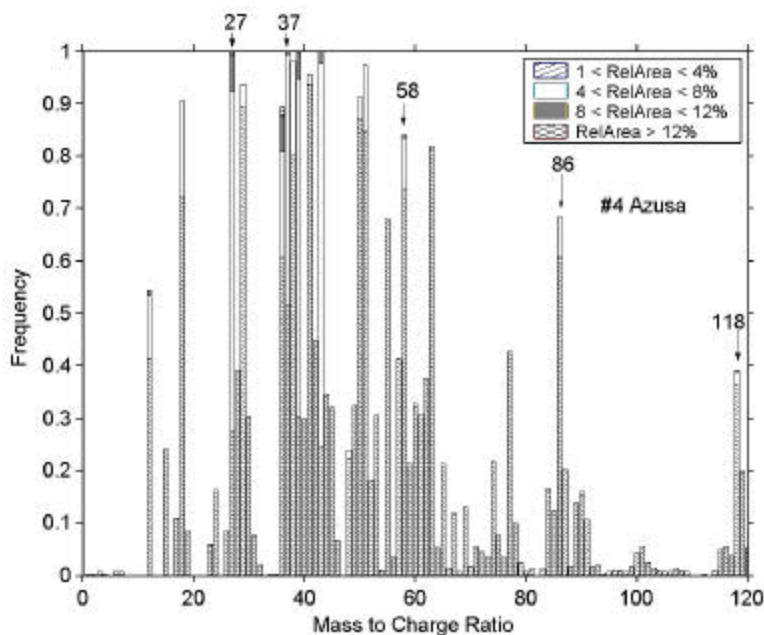


**Figure 3.14: Positive ion “stacked” digital mass spectrum of particles sampled in Azusa, CA on August 21, 1997 and matched to the Riverside cluster 4 organic carbon with amines. These particles are part of the same air mass as those sampled in Los Angeles (see Figure 3.13).**

### 3.3.5 Dual ion ART-2a Analysis with a Higher Vigilance Factor for Trajectory 1

Due to issues involved in matching dual ion spectra from the transportable instruments to the Riverside single polarity clusters and the indication that the classes could be sub-divided to more accurately classify the particle populations in Los Angeles and Azusa trajectory 1, the data were re-analyzed using ART-2a with dual ion spectra as inputs and an increased vigilance factor to require more similarity among particles in each class. The Los Angeles data were used to create clusters and the Azusa data were matched to the resulting weight matrix. At a vigilance factor of 0.6, Los Angeles dual ion data generated 18 clusters (counting only those classes with 10 or more particles). These 18 clusters accounted for 94% of the total particles in Los Angeles and 87% of the Azusa particles matched these classes.

Using a higher vigilance factor of 0.7, Los Angeles dual ion data generated 20 clusters with 10 or more particles (see Appendix F). These 20 clusters accounted for 88% of the particles in Los Angeles and 70% of the Azusa particles matched these classes. A higher vigilance factor created classes that were specific enough to include the early air mass composition and tight enough to exclude the aged air mass particle types (Table 3.1). New classes were generated for the particles sampled in Azusa that did not match the Los Angeles classes (Table 3.2 and Appendix G). The positive ion spectra for the new classes look very similar at both sites—the primary difference is the addition of corresponding negative ion spectra in Azusa, showing contributions from sulfates and nitrates. This is most likely an instrumental phenomenon, associated with the problems with Los Angeles instrument discussed previously. To examine the potential vehicle influence on particles at these sites, the data from both sites were matched (dual ion, vigilance factor 0.7) to classes generated by car and diesel vehicles, as discussed in Chapter 4.

For approximately half of the classes observed in Los Angeles, no negative ion mass spectra were acquired. This is partly due to the difficulty in generating negatively charged species at high relative humidity levels. Since this was one of the first single particle ambient studies, the deleterious effect of high relative humidity was not known until after this study was complete. Also, it was determined after this study that there were electronics problems with the negative ion side of the mass spectrometer sampling in Los Angeles which reduced the number of spectra. In subsequent studies, particles were dried down to a lower relative humidity (i.e. 55%) to eliminate the effect of relative humidity on the spectra, and increase the number of negative ion mass spectra. For some field studies silica gel filled dryers were used. However, SCOS97-NARSTO was the first dual ion field campaign for the transportable instruments and some instrumental details were still being optimized. For the most part, the classes from Los Angeles with only positive ion mass spectra resembled the organic carbon classes, resembling the sub- $\mu\text{m}$  clusters 1 and 2 from Riverside. It is also possible the lower number of spectra was somewhat indicative of lower amounts of secondary processing to produce nitrates and sulfates, two commonly detected negative ions.

The twelfth most common type of particle for Los Angeles had a negative ion mass spectrum but no positive ion mass spectrum. The negative ion mass spectrum for cluster 12 from Los Angeles contained nitrate markers (-46 and -62, and -147 for sodium nitrate). These peaks usually give a strong signal when present.

**Table 3.1. Summary of particle classes identified by ART-2a of dual ion mass spectra from Los Angeles (dual ion, vigilance factor = 0.7). See Appendix F.**

Class	No. in Class	Top 12 Peaks (m/z) Please see the Appendix for a list of m/z values with possible mass spectral peak assignments.												Polarity
1	165	43	37	27	39	38	18	36	50	51	29	41	63	+
		(none)												-
2	124	36	37	43	27	12	39	38	18	50	24	29	30	+
		(none)												-
3	120	23	39	24	63	41	40	62	46	108	25	81	26	+
		(none)												-
4	94	36	12	37	43	27	24	39	38	50	29	18	48	+
		(none)												-
5	88	23	24	39	63	40	62	41	46	108	81	25	26	+
		46	62	24	25	17	16	9	147	131	26	47	35	-
6	72	36	37	12	48	43	24	27	60	38	39	50	29	+
		(none)												-
7	49	23	39	24	41	40	63	43	108	62	57	18	27	+
		62	46	24	25	97	147	125	16	17	26	63	48	-
8	41	23	24	39	40	63	46	62	41	81	25	26	57	+
		24	25	46	16	17	62	41	40	35	1	66	26	-
9	30	23	36	39	37	43	27	24	12	48	41	60	38	+
		(none)												-
10	29	36	60	48	37	43	72	84	61	12	39	49	27	+
		(none)												-
11	18	39	43	18	37	27	36	51	38	29	41	55	12	+
		97	62	46	80	99	98	96	24	26	19	81	41	-
12	18	(none)												+
		46	62	25	17	16	47	35	9	24	147	63	60	-
13	17	43	37	36	18	27	51	39	30	38	12	50	56	+
		62	97	46	125	24	26	80	36	96	19	48	38	-
14	16	39	36	37	27	12	43	38	23	50	51	18	48	+
		(none)												-
15	16	40	57	23	27	24	41	56	1	113	96	39	2	+
		46	62	26	42	17	25	60	9	35	24	48	49	-
16	14	58	37	36	39	38	27	43	12	51	50	18	59	+
		(none)												-
17	11	39	40	41	23	57	56	45	140	64	59	43	18	+
		62	46	41	42	79	125	63	40	147	26	12	148	-
18	11	39	23	40	41	56	43	57	42	24	44	63	27	+
		(none)												-
19	11	55	27	39	23	40	1	24	57	2	41	48	136	+
		46	17	16	26	1	10	62	2	35	3	24	42	-
20	10	51	56	67	58	27	43	39	36	60	37	38	29	+
		(none)												-

**Table 3.2. Summary of additional particle classes identified by ART-2a of dual ion mass spectra from Azusa after matching to Los Angeles (dual ion, vigilance factor = 0.7). See Appendix G.**

Class	No. in Class	Top 12 Peaks (m/z) Please see the Appendix for a list of m/z values with possible mass spectral peak assignments.	Polarity (+/-)
1	42	23 24 39 63 40 46 41 62 81 25 26 64	+
		22 2 3 23 4 5 16 1 6 17 35 15	-
2	40	43 39 27 37 36 18 51 38 58 50 63 86	+
		95 61 42 109 94 96 45 93 78 97 87 60	-
3	39	39 43 27 37 51 18 58 36 38 86 41 29	+
		94 60 42 95 78 96 92 93 86 45 108 41	-
4	26	23 24 63 39 46 40 62 41 81 25 64 26	+
		16 2 17 3 23 22 4 5 1 46 6 35	-
5	21	23 39 24 63 41 62 40 46 81 108 25 92	+
		45 61 16 2 22 60 17 3 34 10 23 9	-
6	21	23 24 39 63 40 62 41 46 25 81 26 108	+
		44 59 15 16 22 2 23 10 40 4 3 60	-
7	13	40 23 41 57 56 39 24 96 44 42 113 59	+
		(none)	-
8	13	56 39 23 27 24 154 41 40 54 138 137 26	+
		46 26 17 35 16 24 25 42 88 37 60 62	-

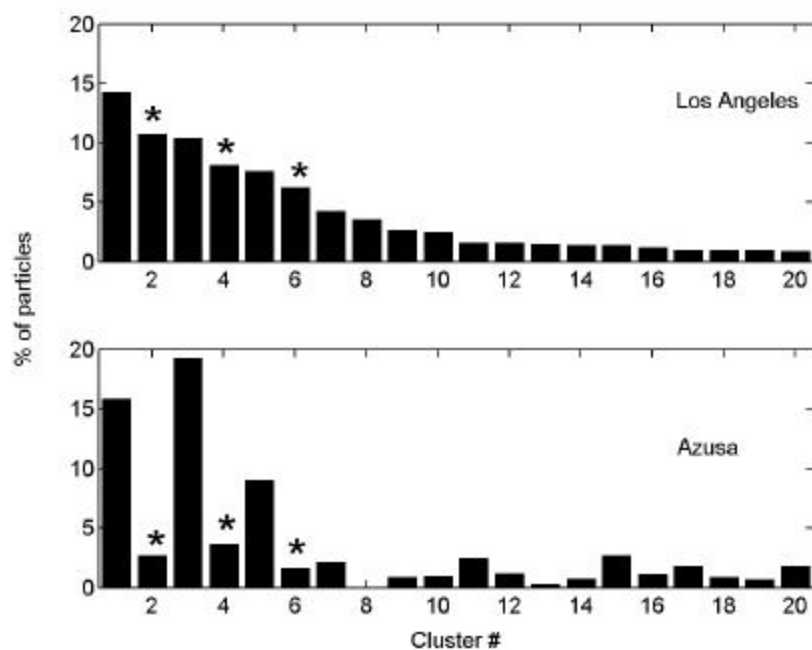


**Figure 3.15: Number of particles per class, identified by ART-2a (vigilance, 0.7; learning 0.05; 40 iterations, classes generated from Los Angeles dual ion data). Particles sampled by the ATOFMS in Los Angeles and Azusa, CA on August 21, 1997. Asterisks above clusters 2, 4, and 6 indicate that they are similar to “freshly emitted” motor vehicle exhaust.**

Interestingly when the Azusa particles are matched to the Los Angeles clusters, a very different distribution among the classes is observed (Figure 3.15). Out of the most common classes for Los Angeles, classes 1, 3, and 5 are also important in Azusa while classes 2, 4, and 6 are detected to a lesser extent than sea salt but still important. In Clusters 1, 3, and 5 are transformed sea salt particles which are over-emphasized due to the transmission bias of the instruments due to the inlet used during this study. Clusters 2 and 4 are both vehicular based and important at both sites. The general particle types appear to be transported and enriched with secondary species between Los Angeles and Azusa. In contrast, other clusters are either diluted or transformed between the two trajectory sites. Clusters 2, 4, and 6 are organic and elemental carbon sub- $\mu\text{m}$  particle types. These particle compositions most likely represent fresh vehicular emissions at both sites. Chapter 4 details the similarity between vehicle tests and these ambient clusters. These clusters found in Los Angeles (cluster 2, 4, and 6) are very similar to car and diesel exhaust particles. Mathematically, the dot product of the weight vectors (the composition of the classes) of two classes can be referred to as the similarity factor. A similarity factor of one would mean the composition of the particle classes was identical. For an ART-2a run at a vigilance factor of 0.7, if the dot product of the particles' vector and a class' weight vector is greater than 0.7, the particle is could be classified into that class. As a preview of the results from vehicle tests and ambient clusters (dual ion ART-2a at a vigilance factor of 0.7) cluster 2 from Los Angeles is very similar to cluster 2 from a car source experiment (similarity 0.8895). Cluster 4 from Los Angeles is nearly identical to cluster 11 from a car source experiment (similarity 0.9717, where 1 is identical) as are cluster 6 from Los Angeles and cluster 27 from a car source experiment (similarity 0.9832). Of the new classes generated in Azusa, classes 2 and 3 are dominated by sub- $\mu\text{m}$  particles (the top right plot in Figures 3.16 and 3.17). These are almost identical to clusters 1 and 2 in Los Angeles except they have the addition of negative ion spectra. This is most likely not atmospherically relevant but due to the Azusa instrument not having the same instrumental difficulties when producing negative ion spectra. The particle mass spectra contain similar peaks in the positive mode and sulfates (cluster 2) and sulfates coupled with nitrates (cluster 3) in the negative ion mode. The amine marker peaks at 86 and 118 stand out in the positive ion weight vector (the top left plot in Figures 3.16 and 3.17). These represent the aged/transformed particles.

The other new clusters detected in Azusa but not Los Angeles are dominated by super- $\mu\text{m}$  particles, and many (such as cluster 7) are dust. The weight vector for cluster 7 includes peaks due to calcium ( $^{40}\text{Ca}^+$ ), iron ( $^{56,57}\text{Fe}^+$ ), and potassium ( $^{39}\text{K}^+$ ). Immediately upwind of the Azusa site is quarry/cement factory that is likely to contribute to the newly observed super- $\mu\text{m}$  particles in the Azusa dataset.

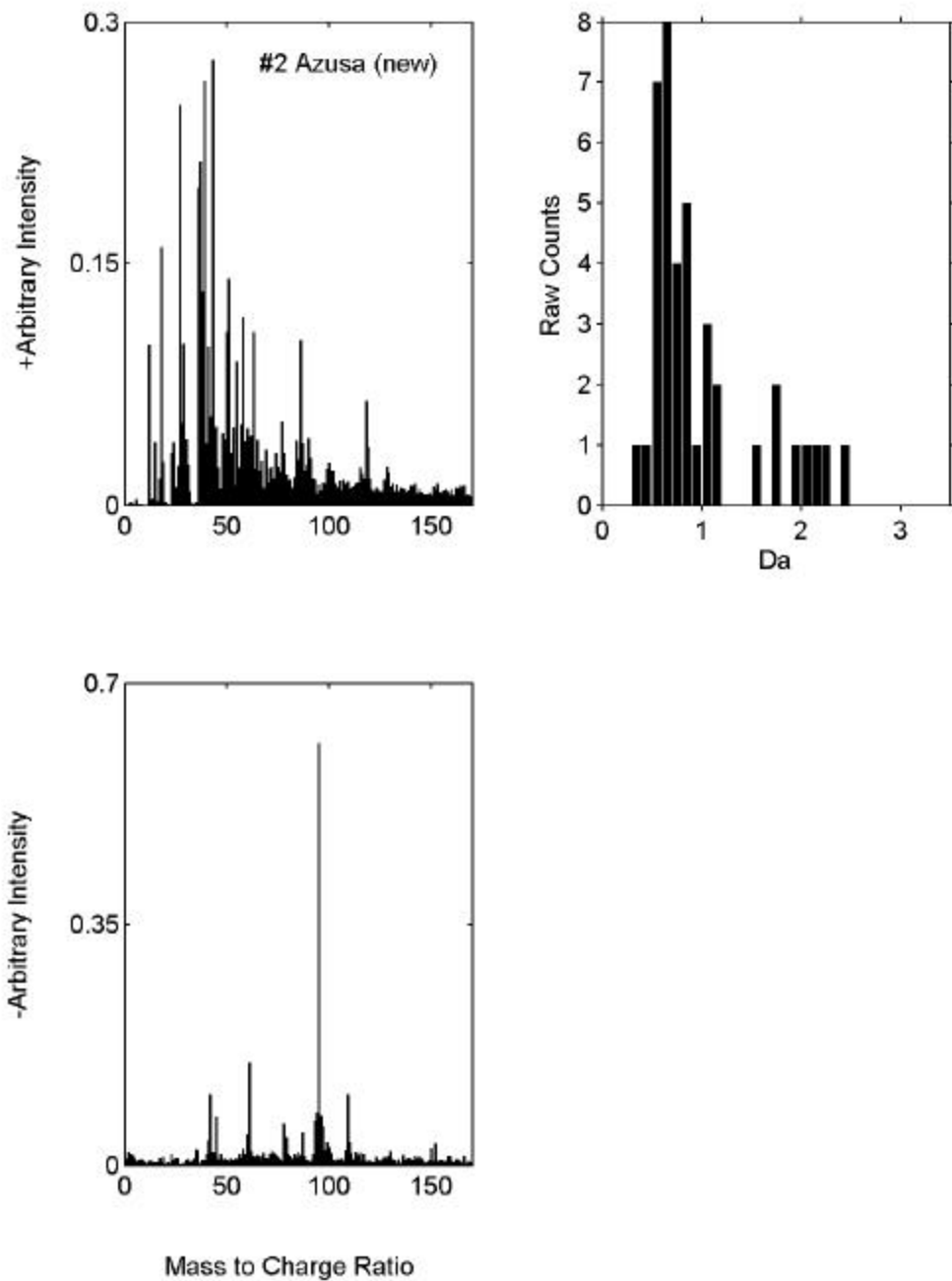


**Figure 3.16: Normalized positive and negative ion weight vector for a newly identified class 2 in Azusa by ART-2a (vigilance, 0.7; learning 0.05; 40 iterations, dual ion data, unlike classes generated using Los Angeles dataset). Particles sampled by the ATOFMS in Azusa, CA on August 21, 1997.**

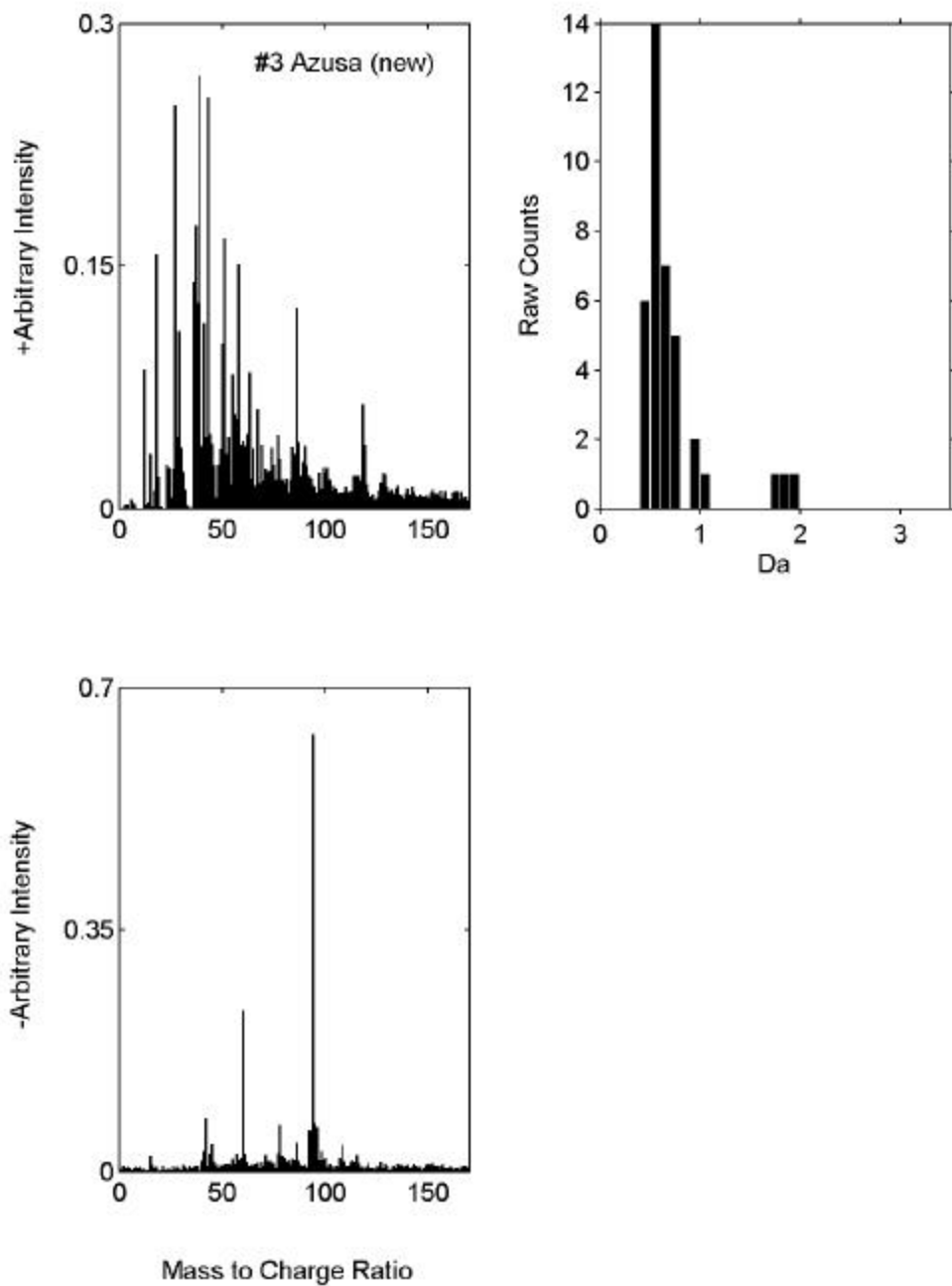


**Figure 3.17: Normalized positive and negative ion weight vector for a newly identified class 3 in Azusa by ART-2a (vigilance, 0.7; learning 0.05; 40 iterations, dual ion data, unlike classes generated from Los Angeles.). Particles sampled by the ATOFMS in Azusa, CA on August 21, 1997.**

### 3.3.6 Nitrate Enrichment during Trajectory 2 Air Mass Transport

Considering  $m/z$  30 as the positive ion marker for nitrate, there was no increase in nitrate for particles transported from Los Angeles to Azusa in trajectory 1. Trajectory 1 traveled quickly in off the Pacific Ocean, rapidly made its way to Los Angeles, and then to Azusa. However, the transported particles for trajectory 2 came quickly in off the Pacific Ocean, rapidly made their way to Los Angeles, stagnated between the sites, and then arrived in Azusa on the following day. The trajectory 2 particles showed increased nitrate (see Figures 3.18 and 3.19, “nitrate-rich” particles mass spectra have an area  $> 500$  at  $m/z$  30). There is a diurnal rise and fall of the nitrate-rich particles over this period. The valleys seem to correlate with fresh marine air masses. The mean area and relative area of the peak at  $m/z$  30 increased from Los Angeles to Azusa for trajectory 2.

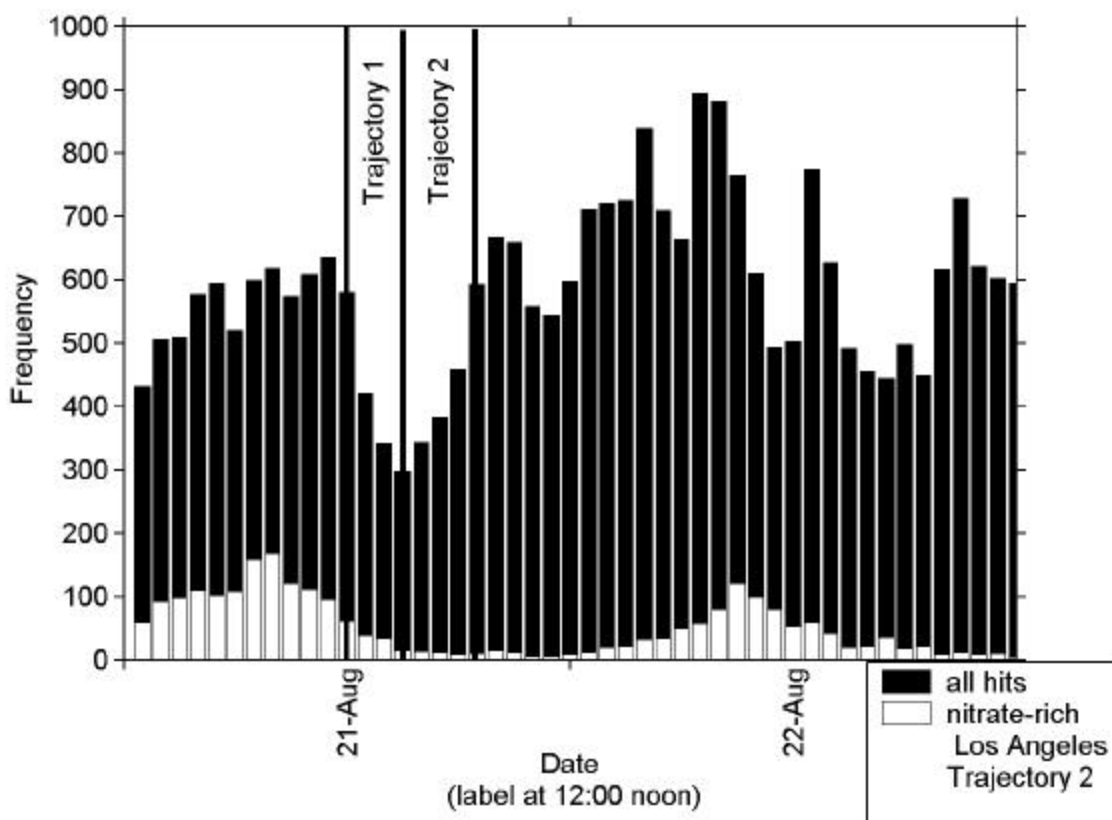
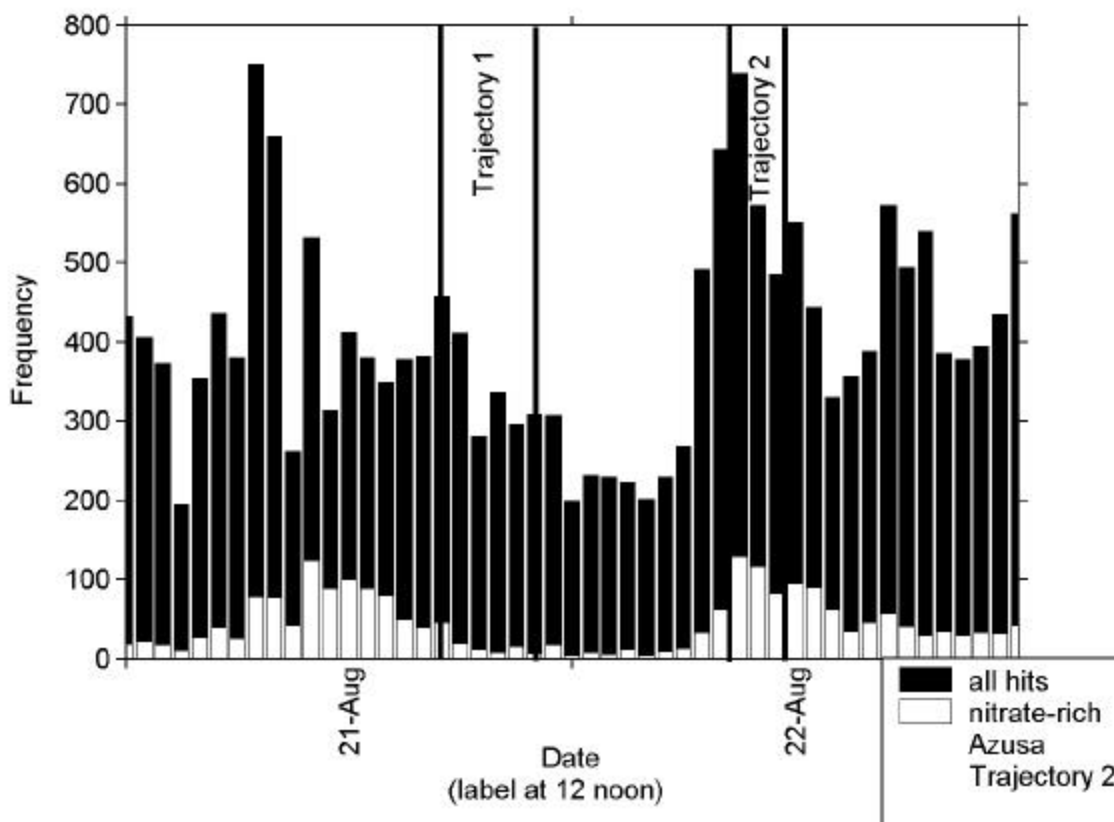


Figure 3.18: Time series plots of all particles with mass spectra sampled in Los Angeles, CA on August 21-22, 1997. The fraction of the total particles in each hour with a peak at  $m/z$  30 (area  $> 500$ ) is shaded in white. Temporal resolution is 60 min. The times for the two transport trajectories are labeled.



**Figure 3.19: Time series plots of all particles with mass spectra sampled in Azusa, CA on August 21-22, 1997. The fraction of the total particles in each hour with a peak at  $m/z$  30 (area > 500) is shaded in white. Temporal resolution is 60 min. The times for the two transport trajectories are labeled.**

The positive ion “stacked” digital mass spectra are shown for particles in Los Angeles and Azusa, trajectory 2 times, in Figure 3.20 and 3.21. These positive ion “stacked” digital mass spectra show less than 8% of the Los Angeles particles had an area greater than 500 at  $m/z$  30, compared to over 22% of the particles in Azusa. The overnight stagnation of the air mass between the two sites allowed for nitrate enrichment that was not observed for particles in the faster moving air mass. The negative ion “stacked” digital mass spectra show an increase in the peaks at  $m/z$   $^{46}\text{NO}_2^-$  and  $^{62}\text{NO}_3^-$  an observation that is consistent with nitrate enrichment.

Other particle composition changes are also evident. The Los Angeles positive ion “stacked” digital mass spectrum looks like a basic sea salt spectrum with peaks of  $^{23}\text{Na}^+$ ,  $^{39/41}\text{K}^+$ ,  $^{40}\text{Ca}^+$ ,  $^{62}(\text{Na}_2\text{O})^+$ ,  $^{108}(\text{Na}_2\text{NO}_3)^+$  and  $^{165}(\text{Na}_3\text{SO}_4)^+$ . The Azusa positive ion “stacked” digital mass spectrum also contains the common sea salt peaks as well as many other peaks. Of note is the decrease in peaks due to sodium chloride at  $m/z$  81 and 83 and the increase in the abundance of  $m/z$  108  $(\text{Na}_2\text{NO}_3)^+$ , indicating the transformation process of  $\text{NO}_x$  with sea salt has occurred during transport. Other additional components of the Azusa aerosol include ammonium  $^{18}(\text{NH}_4)^+$  and nitrate  $^{30}(\text{NO})^+$ . The peak at  $m/z$   $^{97}\text{HSO}_4^-$  in the negative ion “stacked” digital mass spectrum indicates an increase in sulfate. Organic carbon ( $m/z$  27, 37, and others), amines ( $m/z$  58, 86,

and 118), and metals (such as iron  $^{56,57}\text{Fe}^+$ ) also increase for trajectory 2 particles as they are transported between Los Angeles and Azusa.

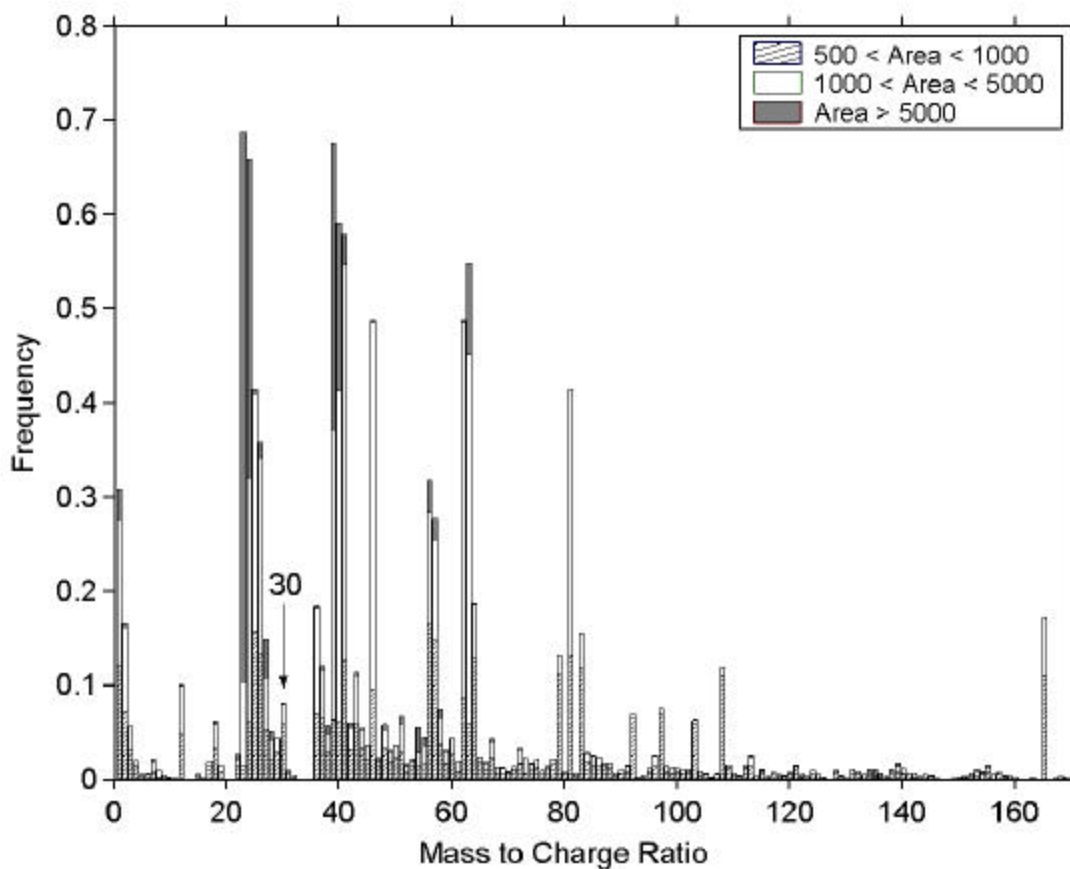


**Figure 3.20: Positive ion “stacked” digital mass spectrum of particles sampled in Los Angeles, CA on August 21, 1997 15:30-18:30.**

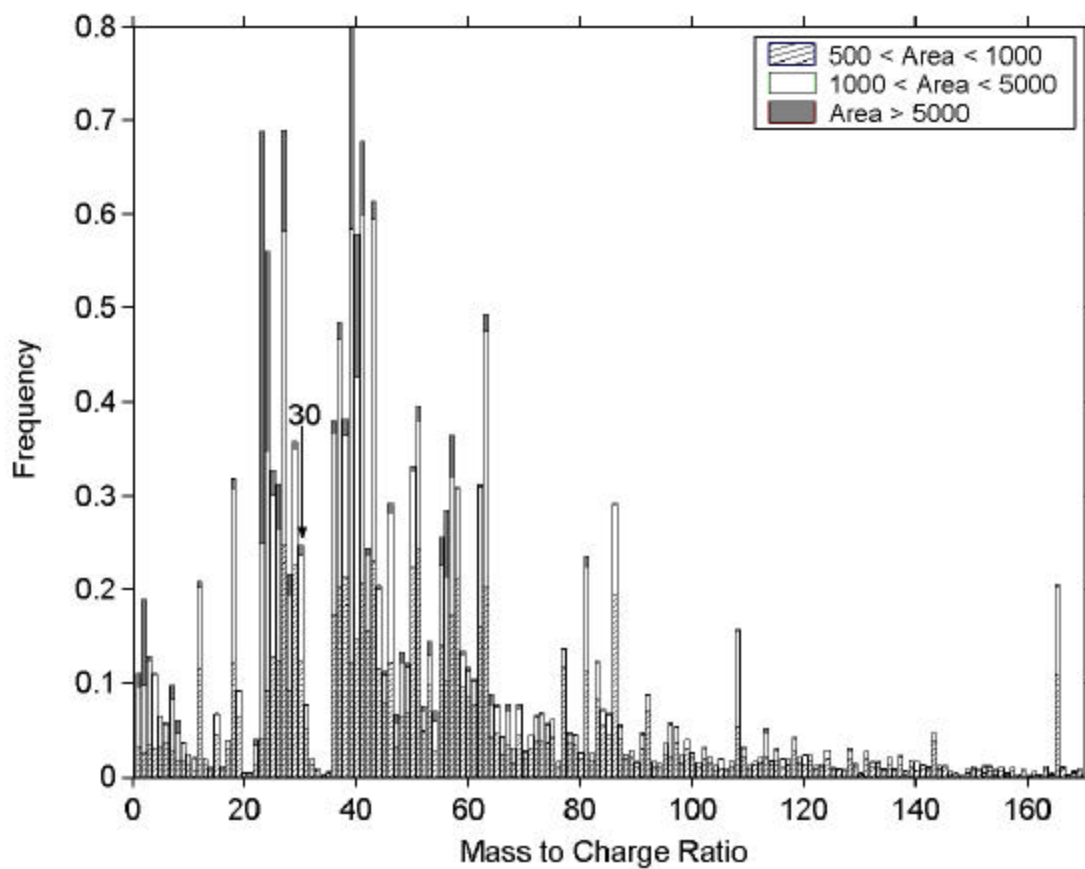


**Figure 3.21: Positive ion “stacked” digital mass spectrum of particles sampled in Azusa, CA on August 22, 1997 8:00-11:00.**

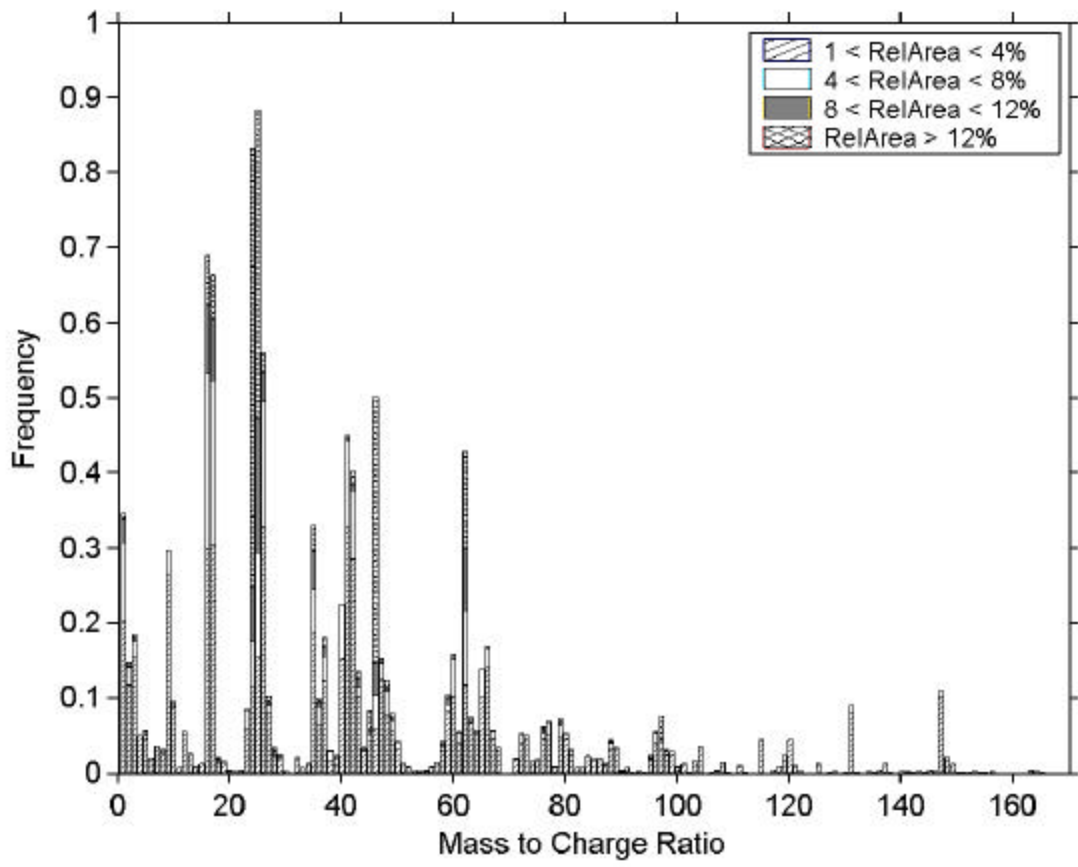


**Figure 3.22: Negative ion “stacked” digital mass spectrum of particles sampled in Los Angeles, CA on August 21, 1997 15:30-18:30.**

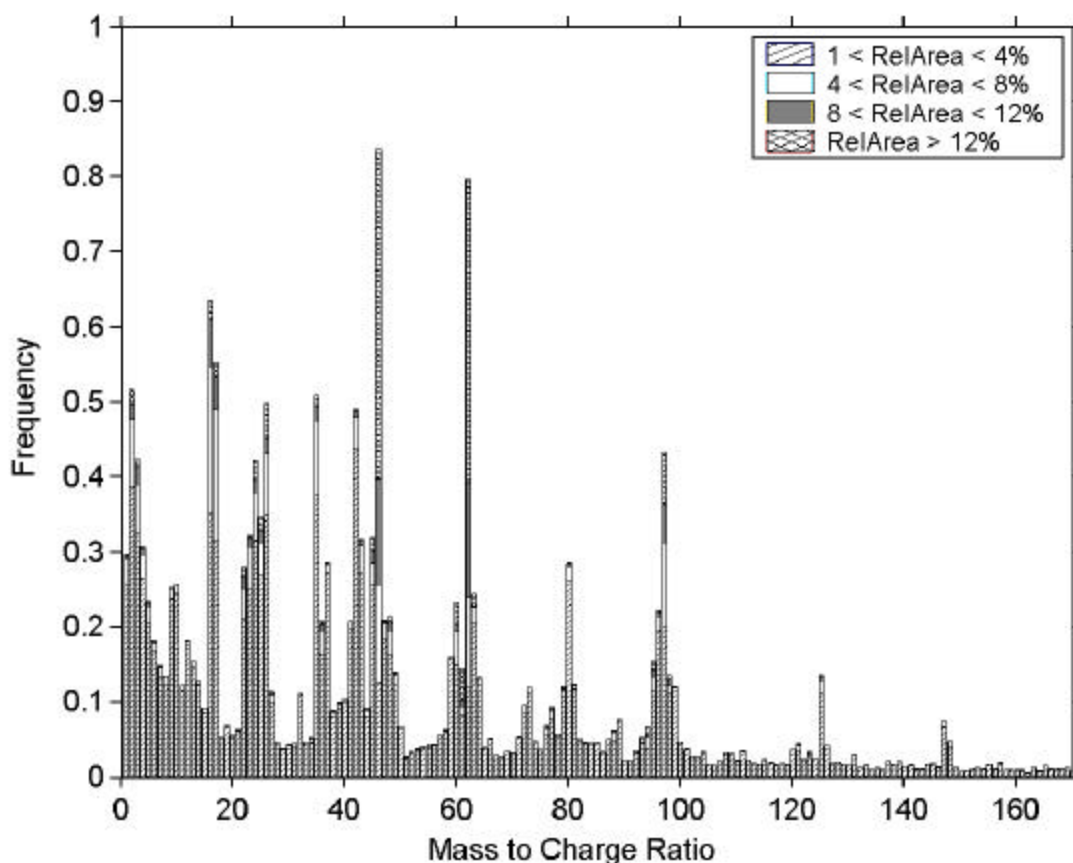


**Figure 3.23: Negative ion “stacked” digital mass spectrum of particles sampled in Azusa, CA on August 22, 1997 8:00-11:00.**

### 3.4 Conclusions

Two different types of transport of air parcels from Los Angeles to Azusa occurred during August 21-22– direct and transport with stagnation. Digital mass spectra and matching using neural network generated clusters were used to compare the particle populations at the two sampling sites. The digital mass spectra indicate the appearance of new peaks, such as the amine markers at  $m/z$  86 and 118 as the general particle types in the air mass from Los Angeles were analyzed in Azusa for trajectory 1.

For trajectory 1, the neural network matching technique generated for sub- and super-  $\mu\text{m}$  particles showed some interesting qualitative trends. The size-composition relationships of the particle classes observed in Riverside persisted in both Los Angeles and Azusa. The sub-  $\mu\text{m}$  particles were most often classified into clusters 4, 11, and 16. The finding that Azusa particles were more commonly classified into cluster 4, organic carbon with amines, is consistent with the digital mass spectra. The Los Angeles site was characterized by more elemental carbon cluster 16 particles, consistent with emissions from vehicles and the fact that several freeways were in close proximity to the sampling site. The super-  $\mu\text{m}$  particles were most often classified into sea salt clusters 1 and 2. Also of note was the soil dust presence in Azusa, most likely enhanced by quarry activity occurring adjacent to the sampling site.

A dual ion ART-2a analysis at a higher vigilance factor was able to more fully characterize the Los Angeles and Azusa aerosols and determine the new classes. Some of the Los Angeles types that were much less common in Azusa were indicative of fresh vehicle emissions. New clusters, such as the ones with strong amine signatures, were identified in the Azusa dataset. The results were somewhat complicated by the fact that the Los Angeles instruments detected less negative ions due to instrumental difficulties. Therefore, some of the new types resembled the Los Angeles types with the addition of negative ion spectra.

For trajectory 2, particles in the air mass were enriched with a variety of species including nitrate, sulfate, organics, metals, and amines. The overall trends of nitrate-rich particles plotted along with the hit particles in Figures 3.18 and 3.19 and the “stacked” digital mass spectra for the trajectory times were presented in Figures 3.20-1.23. These plots show how the stagnation event dramatically changed the composition of the air mass.

By examining the air mass trajectories, obtained after the study, these two trajectories were selected to capture two distinct air mass transport patterns. The sampling times of the filter-based methods (including the MOUDI we use for scaling) captured the fast-moving air mass transport, including trajectory 1. However, the filter-based method failed to capture any transport pattern like trajectory 2 because predictive tools were being used to “guess” when the transport processes of interest would occur. However, as demonstrated here, in real-time the changes in the particles can be observed at the sampling sites using the ATOFMS instruments. In future studies, we plan to use ATOFMS instruments to determine when to sample intensively with filters for comparison. Using real-time changes in the ATOFMS data will ensure that the episodes of the desired chemistry are captured.

## Chapter 4

# Source Characterization

### 4.1 Introduction

Possibly the biggest strength of single particle mass spectrometers lies in their ability to detect unique mass spectral signatures. A goal of ATOFMS studies is to use these signatures to identify particles from different sources and/or particles that undergo processing in the atmosphere. In this chapter, a first attempt is made to make a comparison between ambient particles and source characterization data. Specifically, the ATOFMS data from the SCOS97-NARSTO study are compared to the single particle ATOFMS data obtained in vehicular source characterization studies. In 1998, particles were collected from vehicles while they were run through the Federal Test Procedure (FTP) urban driving cycle on a chassis dynamometer at the California Air Resources Board (CARB) Haagen-Smit Laboratory in El Monte, CA. A dilution tunnel system was used to simulate the typical dilution and cooling conditions of the exhaust from the vehicle before being sampled by the ATOFMS instrument. Using the ART-2a neural network, particles were classified and the “fingerprints” or chemical signatures of the vehicle emission particles determined. Single particle mass spectra acquired during SCOS97-NARSTO were then searched to determine whether the identified source mass spectral “fingerprints” could be detected in ambient samples. This chapter focuses on the application of matching source data to ambient datasets. Ambient datasets of single particle mass spectra contain particles similar to those collected during the vehicle source characterization studies. One should keep in mind that this represents a first attempt to compare a very limited source characterization dataset. The goal is to determine whether source characterization datasets resemble particles detected in ambient air. Further source tests are necessary to fully identify single particle signatures from different sources.

### 4.2 Experimental methods

As discussed in Section 2.3, ATOFMS was used to characterize individual ambient aerosol particles. The data are calibrated for size and the flight time axes are converted to  $m/z$  (see Section 2.3 for details) and compiled in the YAADA database. Rather than create new classes or clusters from ambient particles (as previously demonstrated in Chapter 2), particles emitted from the specific source of interest are used to create classes or signatures that ultimately can be used to identify the source in the atmosphere. The ambient data are then matched to the source-specific classes. The source particles were identified in of data collected at the California Air Resources Board dynamometer facility in El Monte (Suess et al., 2002). The car (light duty vehicle) data include the mass spectra from approximately 1300 particles, sampled from 10 vehicles. The diesel dataset contains mass spectra for approximately 400 particles sampled from a single, medium-duty diesel vehicle. *It is important to note that this dataset represents only a limited sample of the vehicle fleet and further vehicle characterization studies are currently underway with ATOFMS.* In these newer studies, we have determined that the observed particle

types show limited similarities to ambient particles due to issues in the dilution sampling. However, the demonstration of the application of ART-2a to this dataset is an important first step in source apportionment. Matching ambient particles to source particle classes from the dynamometer identifies the ambient particles with similar compositions to particles from the vehicle tests (analogous to the class matching technique demonstrated previously in Chapter 3).

The SCOS97-NARSTO sampling sites for ATOFMS are expected to be impacted by the particle emissions from motor vehicles. In particular, the Los Angeles sampling site was located near several major freeways and thus the particles sampled are expected to have a “fresh emission” character (as briefly discussed in Chapter 3). The Azusa site was located close to freeways and major diesel traffic and thus is expected to show a mixture of fresh vehicular emissions as well as more aged particle types. The inland sites at Riverside should show particles with more “aged” characteristics.

The basic parameters used for the ART-2a analysis include: a range of vigilance factors (0.5, 0.6, 0.7, 0.8, 0.9), a learning rate of 0.05, a maximum of 20 iterations, and the first 350  $m/z$  ( $m/z$ ) units of the mass spectra for creating the vectors. Some of the data were processed using both positive- and negative ion mass spectra, and others using positive ion mass spectra only. The transportable ATOFMS instruments provided dual ion data from the ambient and source studies. The lab-based (Riverside) ATOFMS instrument has only single ion capabilities. Therefore, when data from the transportable instruments are analyzed, both positive- and negative ion mass spectra are considered, however for the Riverside site where the lab-based ATOFMS sampled, it is only possible to use the positive ion data. In some cases, the vigilance factor was increased to refine the specificity of the classes created by ART-2a (i.e. how close the particle ion signatures must resemble another particle type in order to be matched to that class). Results are presented for ART-2a with the vigilance factors of 0.5 to 0.9 and 40 iterations.

One can use ART-2a to mathematically compare the clusters to determine how similar they are to one another. When matching the ambient dataset to the source classes, it is important that the same vigilance factor used for the creation of the clusters by ART-2a analysis be used for both the source and the ambient datasets. The vigilance factor can be thought of as the degree of variability allowed for the particles in a single class. When a particle mass spectrum falls within the specified vigilance factor, it is considered matched to that cluster. When similar clusters exist or a loose vigilance factor is used, a particle may fall into multiple clusters. One can “match” the ambient particles to the clusters exclusively (i.e. if it falls within the vigilance factor of more than one cluster, the particle is placed in only one cluster, the best match) or non-exclusively (if it falls within the vigilance factor of more than one cluster, the particle is placed in all of the clusters, creating duplicates of the particle in multiple classes). For Section 4.3.1, particles are matched exclusively to ensure that each particle is classified into only one class (the best fit for that particle). Matching to the positive ion only set of classes (vigilance factor 0.5) requires exclusive matching or a particle may be matched to a number of classes, making the results difficult to interpret. For Section 4.3.3, we matched particles in a non-exclusive fashion because the data (and classes) are dual ion. When dual ion data are analyzed with a 0.7 vigilance factor, the particles are likely to be classified into only 1-2 classes and the data are straightforward to interpret without forcing each particle’s match to be exclusive.

## 4.3 Results and Discussion

### 4.3.1 Positive ion ART-2a of Dynamometer Source Particles and Chemical Class Comparison to Riverside Ambient

In order to understand the effect of the vigilance factor on the data analysis, vigilance factors of 0.5, 0.6, 0.7, 0.8, and 0.9 were tested. As described above, the vigilance factor was adjusted to change the required similarity between the particles grouped in the same cluster. A tight vigilance factor, such as 0.9, requires the particles to be nearly identical and generates a much larger number of classes than a lower vigilance factor. For example, there are 28 classes from the car dataset when ART-2a is run at 0.9, 24 at 0.6 and only 20 at 0.3 (counting only clusters containing greater than or equal to 0.7 % of the particles, using both positive- and negative ion mass spectra). It has been noted that when the vigilance factor gets relatively high ( $\geq 0.8$ ), ART-2a begins to create classes that are due mostly to inherent shot-to-shot variability imposed by laser beam inhomogeneities in power (i.e. not necessarily related to differences in particle composition). This chapter will focus on the results using a vigilance factor of 0.5 for Riverside and 0.7 for Los Angeles and Azusa, to allow for comparisons to the data presented in the other chapters of this report. The vigilance factor of 0.5 was sufficient to create general positive ion classes for the Riverside particles (see Chapter 2). A higher vigilance factor was adopted for the Los Angeles and Azusa sites in order to observe more subtle composition changes as discussed in Chapter 3.

The lowest vigilance factors tested for the dynamometer data was 0.5. Table 4.1 summarizes the results of the ART-2a analysis using this vigilance factor on the positive ion diesel data from the dynamometer (the negative ion mass spectra were not considered at this stage of the analysis). The positive ion ART-2a weight vectors for clusters 1-6 explain 82% of the particles. The particle types are briefly described in this table. One should note that this ranking is based on unscaled ATOFMS data so no weight should be assigned to the relative ranking as smaller particles are under-counted. Furthermore, only clusters 1-3 have significant particle counts and the signatures of these particle types are very similar to the particle mass spectra observed in ambient air. Recent source tests have determined Cluster 1 and 6 from the diesel tests show a common organic carbon pattern (peaks at 27, 29, 37>36, 50, 51) more typically observed for gasoline than diesel vehicles. There are two possibilities for this observation, 1) the medium duty vehicle used for the tests was not representative of heavy duty vehicles and produced higher amounts of semivolatile organic carbon species, or 2) the dilution conditions used in these experiments caused a higher partitioning of organic species to the particles that typical for diesel emissions. Whatever the reason, it is important to note the overall comparison of ATOFMS source and ambient datasets is limited by the small dataset obtained in this initial source test.

Cluster 5 is similar to an ash particle type observed in ambient studies, including a study alongside a freeway on one performed in the Caldecott Tunnel. Based on recent findings in ATOFMS source tests, the positive ion spectrum is most likely coupled with phosphates and sulfates in the negative ion spectra. The degree of similarity between the classes/clusters can be calculated and plotted. Mathematically, ART-2a generates a set of characteristic mass spectra (the weight matrix), one for each class (a weight vector represents a numeric representation of the characteristic mass spectrum for that class of particles). Each class or cluster is represented by a single weight vector. This vector has 350 numbers. Each number in the vector corresponds to the normalized area under the peaks at a given  $m/z$ . The dot product of the weight vectors is

used to mathematically calculate the similarity of two classes. As verification, a comparison can be made between two identical weight matrices – comparing the positive ion diesel classes to themselves (vigilance factor of 0.5). The dot product for two identical weight vectors is 1. In the resulting plot, the dot product is represented by a shade of gray on a white to black gray-scale. A bright white square (= 1) appears where each weight vector is compared to itself, forming a diagonal from the upper left to lower right corners (Figure 4.1; Appendix P shows color version). The weight vectors for the positive ion diesel data (vigilance factor of 0.5) are compared to one another in the remainder of the matrix and plot. The highest dot product was 0.5542 for clusters 1 and 3. This is not really a close match as these two particle types are quite distinct. In general, based on experience with many single particle datasets, one should note that a dot product of less than 0.8 indicates the particle types are not very similar. The squares where clusters 1 and cluster 3 overlap are medium gray in color. The weight vectors of these two carbon-containing clusters have many peaks in common including peaks at  $m/z$  12, 27, 36-39, and 43 (Table 4.1 and Appendix H). The next highest dot product between clusters is only 0.4698 for clusters 2 and 5. Both of these particle types are dominated by calcium peaks (Table 4.1).

**Table 4.1. Summary of particle classes identified by ART-2a of positive ion mass spectra from the diesel vehicle dynamometer experiment (vigilance factor = 0.5, single polarity analysis). See Appendix H.**

Class	No. in Class	Top 12 Peaks ( $m/z$ ) Please see the Appendix for a list of $m/z$ values with possible mass spectral peak assignments.												Brief Description
1	102	27	37	39	86	43	36	18	12	38	58	29	50	organic carbon, amines
2	90	40	36	41	12	24	56	37	23	57	96	27	44	calcium-rich, carbon
3	74	36	12	40	37	24	27	48	39	60	43	38	23	elemental carbon, calcium-rich
4	28	39	40	23	41	43	27	37	140	55	36	26	58	potassium-rich
5	22	40	57	23	24	42	44	45	58	43	27	65	64	calcium-rich
6	10	51	67	27	56	39	43	37	18	36	12	86	38	vanadium-rich, carbon

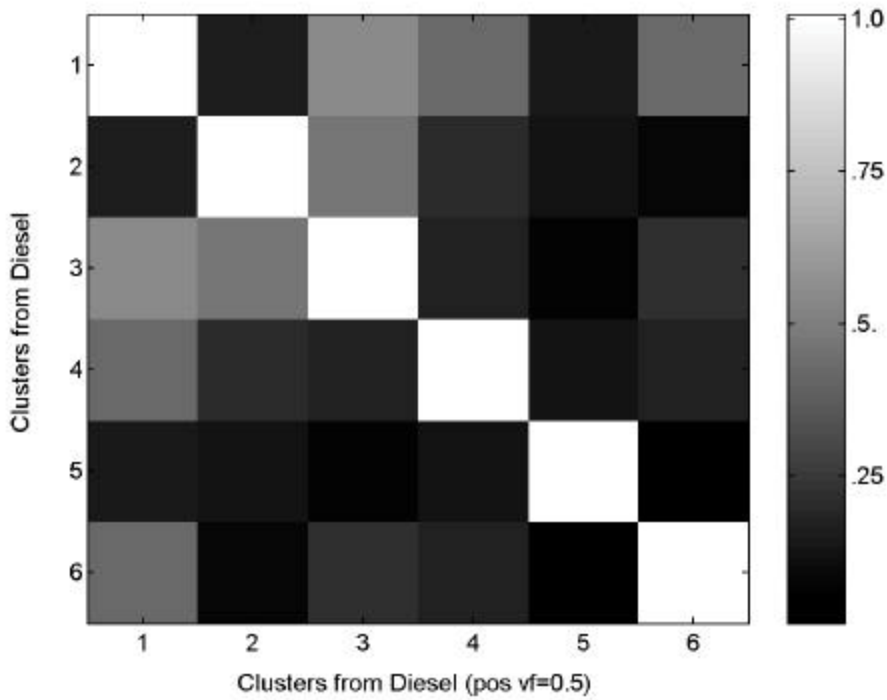


**Figure 4.1: Similarity plot for weight matrices from diesel dynamometer (vigilance factor 0.5). See Appendix O for color version.**

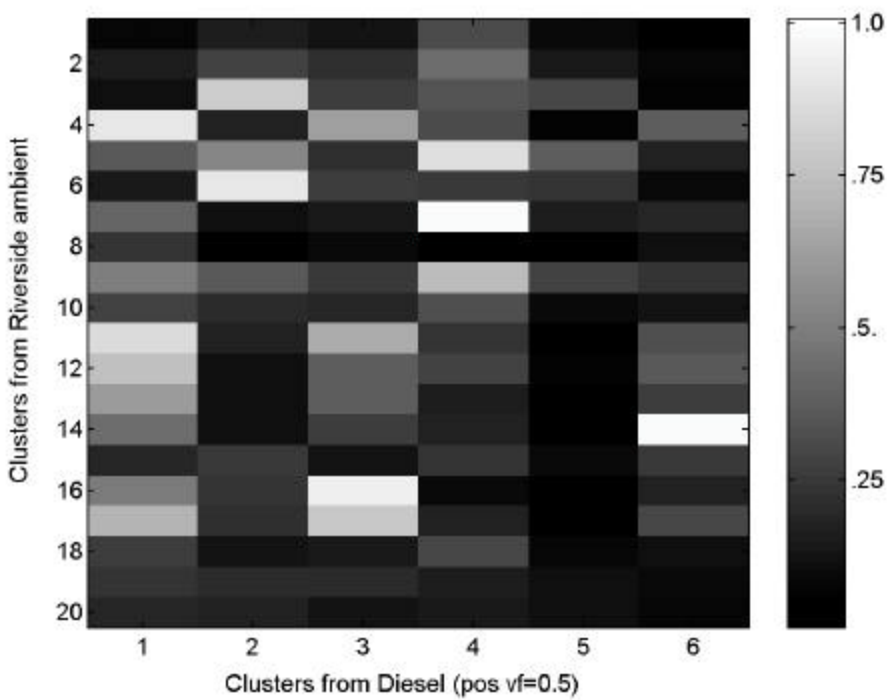


**Figure 4.2: Similarity plot for weight matrices from Riverside ambient and diesel dynamometer (both at vigilance factor 0.5). See Appendix O for color version.**

This same comparison can be made between with the positive ion diesel data (vigilance factor of 0.5) and the Riverside ambient clusters (discussed in Chapter 2). Figure 4.2 (see Appendix P for color version) shows the degree of similarity between clusters in the ambient analysis (top 20 clusters) and the diesel analysis (6 clusters). For clusters that are similar, the dot product (only those >0.8 are listed) and some of the peaks in common are included in Table 4.2. By picking out clusters that are similar between two datasets, the interpretation of the data is simplified. Classes with similarities and differences can readily be identified. For example, Riverside cluster 14 and diesel cluster 6 are nearly identical, with a similarity of 0.9863 (identical particle clusters have a similarity of 1.0). One expects the temporal and size patterns of diesel cluster 6 to be nearly identical to Riverside cluster 4 because many of the same particles will be in the two classes. Connections (or lack of) between the particle composition in the two datasets are also quickly realized. For example, it is interesting to note that none of the Riverside ambient clusters have a close similarity to cluster 5 from the diesel dynamometer test (0.3705 is the highest dot product).

**Table 4.2. Summary of similarity between particle classes identified by ART-2a for positive ion mass spectra from the diesel vehicle dynamometer experiment and the ambient experiment in Riverside (vigilance factor = 0.5).**

Dot Product (Similarity)	Diesel Dynamometer Cluster	Riverside Ambient Cluster	Major peaks in common, by <i>m/z</i> (See Tables 4.1 and 2.1) See the Appendix for more on <i>m/z</i> values.
0.9863	6	14	12 18 27 37 38 39 43 51 67
0.9847	4	7	23 27 36 39 40 41 43
0.9345	3	16	12 23 24 27 36 37 39 43 48 60
0.9099	1	4	12 18 27 29 36 37 38 39 43 86
0.9084	2	6	23 24 27 40 41 44 56 57 96
0.8806	4	5	23 27 39 40 41
0.8589	1	11	12 18 27 36 37 38 39 43 50 86
0.8013	2	3	23 24 36 40 41 44 56 57

It is also interesting to note when multiple Riverside ambient clusters are quite similar to single diesel dynamometer clusters. For example, Riverside clusters 5 and 7 both resemble diesel cluster 4 and share many characteristic marker peaks. It is likely that the Riverside data had a variety of particles with subtle differences that ART-2a grouped together, while the diesel dataset was more homogeneous. The diesel data from the dynamometer represented particles from only one diesel engine and with only minimal dilution and influence from other pollutants. The Riverside data include transformed and aged exhaust particles from a variety of vehicles that were exposed to a wide range of ambient conditions, including various gas-phase species. Later in this chapter, the results for the higher vigilance factor ART-2a are discussed and the Los Angeles and Azusa data are compared to the dynamometer experiments. Table 4.3 summarizes the clusters that are similar in the Riverside ambient and dynamometer diesel datasets (refer to Table 4.2). The table gives the dot product for the cases where two Riverside ambient clusters are similar to a single diesel cluster.

**Table 4.3. Summary of similar classes identified by ART-2a for positive ion mass spectra from the diesel vehicle dynamometer experiment and the ambient experiment in Riverside (vigilance factor = 0.5).**

Diesel Dynamometer Cluster	Riverside Ambient Cluster	Dot Product/ Similarity of Ambient Clusters (pair listed in previous column)	Brief Description
1	4 & 11	0.8601	organic carbon, amines
2	3 & 6	0.8317	calcium-rich
3	16	-	
4	5 & 7	0.8592	potassium-rich
6	14	-	

Simultaneous positive and negative ion mass spectra were obtained for many of the particles analyzed because the dynamometer dataset was taken with a transportable ATOFMS. Once the dual ion dynamometer data was classified using ART-2a (vigilance factor 0.5), it was compared to the SCOS97-NARSTO data from Los Angeles and Azusa (for simplicity, the times compared will be the times discussed in Chapter 3 at these sampling sites). Table 4.4 summarizes the results of the ART-2a analysis on the dual ion diesel data from the dynamometer. ART-2a generates more classes because of the added complexity of the dual ion mass spectra. The dual ion diesel ART-2a weight vectors for clusters 1-12 explain 92% of the particles (vigilance factor 0.5). The classes in Table 4.4 have very little similarity to one another when the dot product is calculated. The most similar dual ion diesel clusters are 3 and 9 with a dot product of 0.7807 for the dual ion weight vectors (Figure 4.3; Appendix P shows color version). This similarity can be attributed to the fact that both particle types show a dominant peak at m/z 40 (Ca). Other peaks in the spectra of the two particle types are actually quite different, however ART-2a can be strongly influenced by one large peak with a high relative area. This is a weakness of the ART-2a analysis scheme that must be recognized when interpreting the results.

**Table 4.4. Summary of particle classes identified by ART-2a of dual ion mass spectra from the diesel vehicle dynamometer experiment (vigilance factor = 0.5, dual polarity analysis).**

Class	No. in Class	Top 12 Peaks (m/z)												Ion
		Please see the Appendix for a list of m/z values with possible mass spectral peak assignments.												
1	61	37	39	27	36	43	86	12	18	58	38	29	50	+
		97	62	125	46	80	96	98	99	63	188	43	64	-
2	53	27	37	39	18	43	86	36	12	38	29	58	50	+
		94	60	121	182	95	45	78	61	21	243	20	93	-
3	42	40	41	36	24	12	56	44	23	37	42	27	64	+
		24	5	25	2	26	36	3	12	48	6	97	16	-
4	39	40	36	12	24	37	27	56	23	47	41	39	38	+
		97	79	24	98	96	46	80	99	26	36	63	62	-
5	31	36	12	37	24	40	27	48	39	43	38	60	18	+

		94	95	77	60	23	96	35	93	78	121	76	45	-
6	30	36	37	40	60	48	12	61	84	23	27	72	24	+
		24	48	36	60	72	25	49	97	96	84	5	26	-
7	25	41	23	24	57	39	42	44	36	45	27	43	37	+
		24	5	25	26	48	36	6	2	49	60	10	3	-
8	24	39	40	23	41	43	140	37	27	36	24	56	12	+
		24	46	62	43	5	42	26	2	94	25	3	41	-
9	22	40	57	36	96	56	41	43	12	37	64	27	44	+
		26	42	46	24	79	48	25	36	43	5	16	49	-
10	19	51	67	58	40	56	59	39	27	57	37	43	60	+
		62	97	46	125	80	96	63	98	99	35	43	64	-
11	11	27	136	39	56	54	153	40	25	55	135	37	38	+
		46	43	10	16	17	62	25	42	9	3	24	26	-
12	10	51	67	27	18	37	43	39	30	38	58	12	19	+
		60	94	121	45	78	77	12	61	106	93	41	62	-

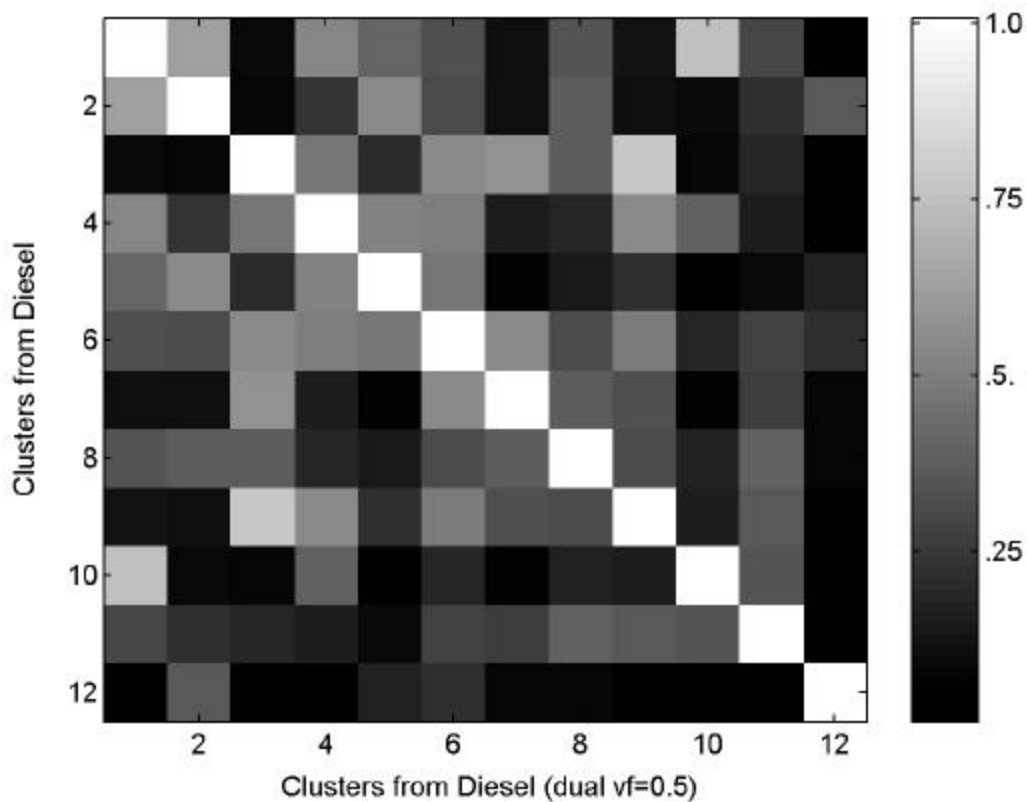


**Figure 4.3: Similarity plot for weight matrices from the dual ion Diesel dynamometer and itself (vigilance factor 0.5). See Appendix O for color version.**

Similarities can be quickly identified between the positive ion and dual ion classes in Tables 4.1 and 4.4, when the positive ion portion of the dual ion data is considered without its negative counterpart. . For example, the positive ion peaks in clusters 10 and 12 in Table 4.4

resemble the vanadium-rich, carbon cluster 6 in Table 4.1. Similarly, the positive ion peaks in clusters 5 and 6 in Table 4.4 resemble cluster 3 in Table 4.1. It is interesting then to look at the differences in the negative ion mass spectra. For clusters 5 and 6 in Table 4.4, the negative ion marker peaks are quite different. Specifically, the negative ion peaks for cluster 6 represent elemental carbon (most important negative ion peaks of carbon envelopes  $^{24}\text{C}_2$ ,  $^{48}\text{C}_4$ ,  $^{36}\text{C}_3$ ,  $^{60}\text{C}_5$ ,  $^{72}\text{C}_6$ ), and the negative ion peaks for cluster 5 are characterized by three large peaks instead the series of carbon envelopes. The three negative ion peaks that characterize cluster 5 are listed as m/z 94, 77, 60 (a series which does not make sense chemically). However, these are probably a miscalibrated set of the peaks and based on other spectra are most likely  $^{63}\text{PO}_2^-$ ,  $^{79}\text{PO}_3^-$ , and  $^{95}\text{PO}_4^-$ . In general, as shown here, obtaining both the positive and negative ion mass spectra enhance the ability to determine different particle types and distinguish between sources. In some cases, one polarity of the mass spectra for two distinct particle types is identical while the other polarity shows distinguishing peaks.

A summary of the classes from the ART-2a analysis of particles emitted from cars on the dynamometer is presented in Tables 4.5 (positive ion) and 4.6 (dual ion). See Appendices J and K for weight vectors. As with the diesel data, similarities can be identified between the classes when the positive ion portion of the dual ion data is considered without the negative counterpart. Compared to the diesel experiment with 6 positive ion only and 12 dual ion ART-2a generated classes, the car experiment yielded more classes, a total of 14 positive ion only and 22 dual ion (vigilance factor=0.5). The car sample included 10 vehicles. The variation between vehicles and the higher overall number of particle spectra sampled help explain why more ART-2a classes were generated for the cars than for the medium duty diesel vehicle.

As with the diesel data, the car source experiment data (vigilance factor=0.5, positive ion only) can be compared to the ambient data from Riverside. Figure 4.4 (see Appendix O for color version) shows a comparison plot. A few nearly white spots are visible indicating the two classes are very similar. Table 4.7 details which classes were the most similar between the datasets. To highlight several matches beginning with the most similar, car cluster 7 resembles Riverside “sea salt” cluster 1, car cluster 8 resembles Riverside “elemental carbon” cluster 16, and car cluster 5 resembles Riverside “potassium-rich” cluster 7. The car cluster 11 resembles Riverside “iron-rich” cluster 15, car cluster 6 resembles Riverside “vanadium-rich” cluster 14, car cluster 9 resembles Riverside “calcium-rich” cluster 6 and so on. As this table shows, a variety of particle types appear to overlap between the car exhaust particles and Riverside ambient classes (at this vigilance factor and with only positive ion data considered). Table 4.8 summarizes the Riverside ambient clusters that are ranked as most similar to the car clusters. The organic-carbon with amine particle type, Riverside ambient clusters 4 and 11, closely resemble the top four car clusters. Other car clusters are similar to the potassium-rich, iron-rich, vanadium-rich, sea salt, and elemental carbon particle classes observed in Riverside.

ART-2a analysis was also run at a higher (tighter) vigilance factor of 0.7 on both the car and diesel dynamometer datasets. This divided the particle types further as shown in Appendices L and M. These types were then compared with particle types observed in ambient air as described in the next section.

**Table 4.5. Summary of particle classes identified by ART-2a of positive ion mass spectra from the car vehicle dynamometer experiment (vigilance factor = 0.5, single polarity analysis). See Appendix J.**

Class	No. in Class	Top 12 Peaks (m/z) Please see the Appendix for a list of m/z values with possible mass spectral peak assignments.											
1	335	27	43	39	37	18	36	38	29	58	12	41	86
2	147	18	58	27	39	43	37	86	36	12	38	29	41
3	134	27	37	43	39	36	29	38	12	41	57	50	55
4	102	36	12	37	27	43	24	39	38	29	18	58	50
5	93	39	41	27	18	43	23	37	40	36	58	12	29
6	90	51	67	43	39	27	37	18	58	23	36	68	56
7	82	23	39	24	40	63	41	27	56	62	37	36	55
8	48	36	12	37	48	60	43	27	24	39	29	38	18
9	35	40	41	24	57	27	56	43	55	23	12	39	37
10	18	54	39	23	40	26	24	27	47	57	62	136	51
11	17	56	24	39	27	40	54	25	23	137	154	41	58
12	12	52	24	38	26	23	55	27	2	37	3	22	39
13	11	38	26	44	53	45	22	2	135	52	136	3	55
14	10	102	58	18	43	27	39	90	37	12	36	29	44

**Table 4.6. Summary of particle classes identified by ART-2a from the car vehicle dynamometer experiment (vigilance factor = 0.5; dual polarity analysis). See Appendix K.**

Class	No. in Class	Top 12 Peaks (m/z) Please see the Appendix for a list of m/z values with possible mass spectral peak assignments.												Ion
1	195	27	37	43	39	36	18	38	29	12	58	41	86	+
		98	49	25	7	9	8	60	63	12	11	36	6	-
2	158	27	43	39	37	18	36	12	58	29	38	86	41	+
		97	62	8	10	7	9	98	12	11	6	99	96	-
3	115	18	58	43	39	27	37	86	29	36	38	12	41	+
		11	12	9	10	13	8	14	15	16	7	17	97	-
4	115	27	37	43	36	12	39	38	29	58	41	57	50	+
		11	10	9	8	12	13	14	15	7	16	17	18	-
5	86	36	12	37	27	24	43	39	48	38	29	18	40	+
		97	12	9	10	8	11	7	13	14	6	15	98	-
6	86	51	67	43	27	39	56	37	18	23	58	68	36	+
		97	10	12	11	9	13	46	8	62	16	14	15	-
7	67	39	41	23	43	27	36	18	40	37	58	12	55	+
		11	10	46	9	97	13	8	7	62	15	14	12	-
8	62	27	39	43	37	18	29	41	58	86	36	38	12	+
		62	97	46	10	9	8	7	11	6	12	13	125	-
9	57	23	39	24	40	63	41	62	46	165	108	56	81	+
		46	62	10	11	9	8	14	12	13	16	17	7	-
10	42	45	73	28	12	37	147	27	36	44	39	74	38	+
		9	11	10	12	13	8	14	15	16	7	17	18	-
11	30	18	58	27	39	37	43	36	12	86	29	38	30	+
		13	10	9	8	16	17	7	11	19	18	15	20	-
12	24	40	57	41	27	43	23	56	39	55	24	37	12	+
		10	12	9	11	8	46	13	14	62	16	15	17	-
13	21	27	43	39	37	36	18	12	29	38	51	41	58	+
		95	61	8	7	9	10	6	11	5	12	4	3	-
14	21	18	64	30	46	66	19	43	68	17	36	36	12	+
		97	62	46	8	7	6	95	10	80	11	9	13	-
15	21	23	39	27	36	24	41	63	40	25	37	56	57	+
		60	79	26	80	63	48	45	36	24	16	17	72	-
16	20	36	60	48	132	43	61	37	84	72	120	23	64	+
		48	60	72	36	24	96	97	84	11	108	10	8	-
17	19	56	39	24	27	40	54	25	23	154	137	41	57	+
		16	46	10	17	35	24	8	3	12	11	26	9	-
18	18	54	39	23	26	24	27	47	40	57	62	51	136	+
		35	17	36	55	54	25	16	52	3	56	18	53	-
19	11	58	27	37	18	36	43	12	39	86	38	29	30	+
		15	10	7	3	5	6	8	4	2	9	21	22	-
20	11	40	24	41	55	56	59	25	57	27	26	23	44	+
		24	26	16	8	10	11	6	25	2	3	79	17	-
21	10	38	26	44	53	45	22	2	52	3	55	135	28	+
		46	62	10	8	63	63	47	89	6	7	7	9	-
22	10	52	24	38	26	23	27	2	37	22	3	36	12	+
		54	53	55	24	56	57	23	58	1	-			

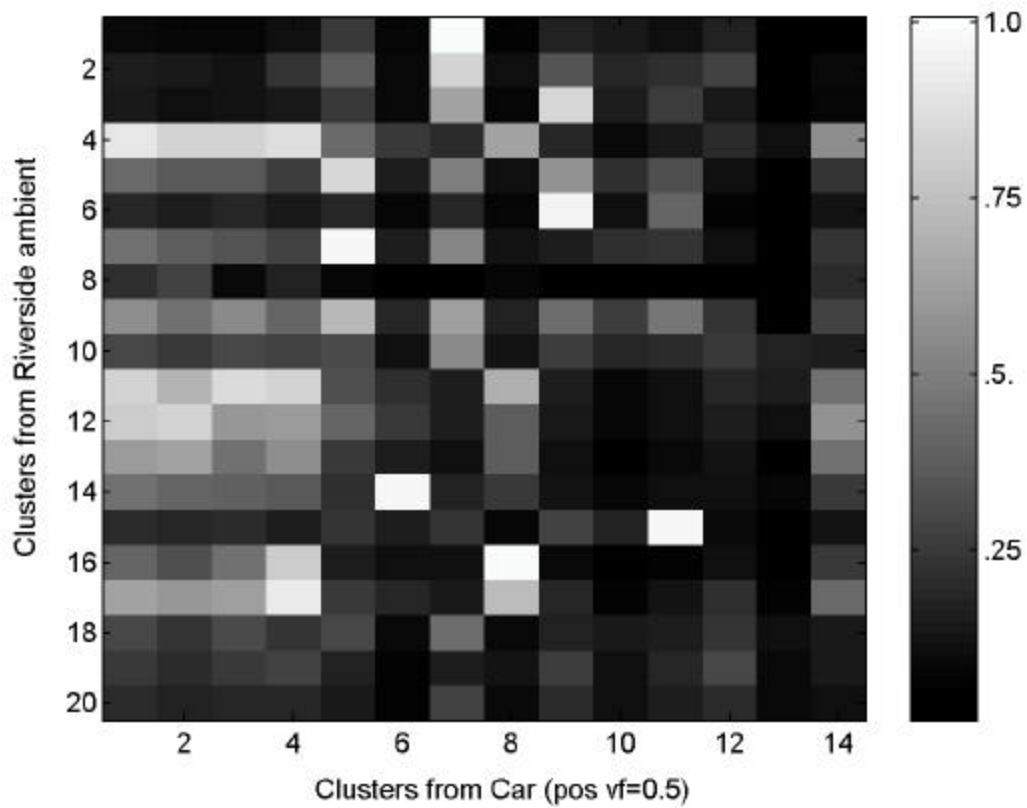


**Figure 4.4: Similarity plot for weight matrices from the Riverside ambient and the positive ion Car dynamometer (vigilance factor 0.5). See Appendix O for color version.**

**Table 4.7. Summary of similarity between particle classes identified by ART-2a for positive ion mass spectra from the car vehicle dynamometer experiments and the ambient experiment in Riverside (vigilance factor = 0.5).**

Dot Product (Similarity)	Car Dynamometer Cluster	Riverside Ambient Cluster
0.9851	7	1
0.9777	8	16
0.9719	5	7
0.9683	11	15
0.9676	6	14
0.9471	9	6
0.9241	4	17
0.9070	1	4
0.8707	4	4
0.8601	3	11
0.8402	9	3
0.8394	5	5
0.8345	2	4
0.8332	3	4
0.8316	2	12
0.8296	7	2
0.8294	4	11
0.8277	1	11
0.8020	4	16

**Table 4.8. Summary of similar classes identified by ART-2a for positive ion mass spectra from the car vehicle dynamometer experiments and the ambient experiment in Riverside (vigilance factor = 0.5).**

Car Dynamometer Cluster	Riverside Ambient Cluster
1	4 & 11
2	4
3	4 & 11
4	4 & 11 & 16 & 17
5	5 & 7
6	14
7	1 & 2
8	16
9	3 & 6
11	15